AEDC TR-97-1

Adaptation of a Three-Dimensional Numerical Simulation to Represent Gas Turbine Engine Compression Systems

Jacqueline C. H. Chalk
Sverdrup Technology, Inc., AEDC Group

April 1997

Final Report for Period September 1, 1995 to December 14, 1996

ARNOLD ENGINEERING DEVELOPMENT CENTER
ARNOLD AIR FORCE BASE, TENNESSEE
AIR FORCE MATERIEL COMMAND
UNITED STATES AIR FORCE

NOTICES

When U. S. Government drawings, specifications, or other data are used for any purpose other than a definitely related Government procurement operation, the Government thereby incurs no responsibility nor any obligation whatsoever, and the fact that the Government may have formulated, furnished, or in any way supplied the said drawings, specifications, or other data, is not to be regarded by implication or otherwise, or in any manner licensing the holder or any other person or corporation, or conveying any rights or permission to manufacture, use, or sell any patented invention that may in any way be related thereto.

Qualified users may obtain copies of this report from the Defense Technical Information Center.

References to named commercial products in this report are not to be considered in any sense as an endorsement of the product by the United States Air Force or the Government.

This report has been reviewed by the Office of Public Affairs (PA) and is releasable to the National Technical Information Service (NTIS). At NTIS, it will be available to the general public, including foreign nations.

APPROVAL STATEMENT

This report has been reviewed and approved.

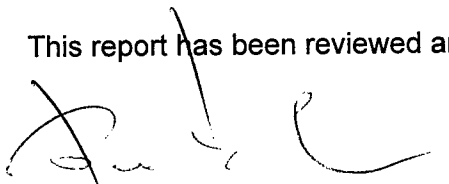

BRIAN D. COLLINS, Capt, USAF
Technology Project Manager
Applied Technology Division
Test Operations Directorate

Approved for publication:

FOR THE COMMANDER

ROBERT T. CROOK
Assistant Chief, Applied Technology Division
Test Operations Directorate

REPORT DOCUMENTATION PAGE	Form Approved OMB No. 0704-0188

1. AGENCY USE ONLY (Leave blank)	2. REPORT DATE	3. REPORT TYPE AND DATES COVERED
	April 1997	Final Report for Period Sept. 1995 - Dec. 1996

4. TITLE AND SUBTITLE

Adaptation of a Three-Dimensional Numerical Simulation to Represent Gas Turbine Engine Compression Systems

5. FUNDING NUMBERS

AF JN 0091

6. AUTHOR(S)

Jacqueline C.H. Chalk
Sverdrup Technology, Inc., AEDC Group

7. PERFORMING ORGANIZATION NAME(S) AND ADDRESS(ES)

Arnold Engineering Development Center/DOP
Air Force Materiel Command
Arnold Air Force Base, TN 37389-5050

8. PERFORMING ORGANIZATION (REPORT NUMBER)

AEDC-TR-97-1

9. SPONSORING/MONITORING AGENCY NAMES(S) AND ADDRESS(ES)

Arnold Engineering Development Center/DOP
Air Force Materiel Command
Arnold Air Force Base, TN 37389-5050

10. SPONSORING/MONITORING AGENCY REPORT NUMBER

11. SUPPLEMENTARY NOTES

Available in Defense Technical Information Center (DTIC).

12A. DISTRIBUTION/AVAILABILITY STATEMENT

Approved for public release; distribution is unlimited.

12B. DISTRIBUTION CODE

13. ABSTRACT (Maximum 200 words)

A new three-dimensional compression system simulation was constructed by coupling the three-dimensional Navier-Stokes flow solver, NPARC, with source terms that model the effects of turbomachinery components. A stage-by-stage characteristic technique adapted from the one-dimensional compressor code, DYNTECC, was used to calculate the turbomachinery source terms. This report discusses the development, adaptation, and implementation of the stage characteristic approach for calculating sources used in NPARC. The distribution of the source terms from the one-dimensional domain to the three-dimensional domain is presented, and an investigation of the radial distribution of the sources during pre-stall compressor performance was conducted. A simple compressor, consisting of a single transonic rotor, was modeled because experimental data were available for comparison.

14. SUBJECT TERMS

compressor, axial flow, modeling, simulation, NPARC, three-dimensional, source terms

15. NUMBER OF PAGES

86

16. PRICE CODE

17. SECURITY CLASSIFICATION OF REPORT	18. SECURITY CLASSIFICATION OF THIS PAGE	19. SECURITY CLASSIFICATION OF ABSTRACT	20. LIMITATION OF ABSTRACT
UNCLASSIFIED	UNCLASSIFIED	UNCLASSIFIED	SAME AS REPORT

PREFACE

The research reported herein was conducted at the Arnold Engineering Development Center (AEDC), Air Force Materiel Command (AFMC). The work and analysis for this research were performed by personnel of Sverdrup Technology, Inc., AEDC Group, operating contractor for the test facilities at AEDC, AFMC, Arnold Air Force Base, TN, under Job 0091. The Air Force Project Manager was Capt. Brian Collins. The manuscript was submitted for publication on February 20, 1997.

CONTENTS

Page

ILLUSTRATIONS

Figure Page

Figure Page

TABLES

APPENDIX

1.0 INTRODUCTION

As modern aircraft gas turbine engines push their operational envelopes, stable aerodynamic operation of the engine's components is imperative. The compression system delivers a desired airflow and pressure rise at a specified rotational speed during normal operation. Compression system performance influences the performance of all other engine components. For many gas turbine engines, the compression system consists of one or more aerodynamically coupled axial compressors. An axial compressor is comprised of stages containing a rotating component, or rotor, and a stationary component, or stator. The rotor is a circumferentially arrayed series of airfoils on a disk which, when rotating, imparts kinetic energy to the fluid. The rotor and/or stator diffuses the flow, creating pressure rise. In addition, the stator redirects the flow for the next stage. The compressor, powered by work extracted by the turbine, increases the pressure of the airflow before it enters the combustor. This increase in pressure of the incoming air increases the net energy available from the gas generator. However, the engine compression system can be susceptible to non-uniform flow conditions at the engine inlet which may force the compressor into unstable operation.

During steady-state operation, the compressor operates at some nominal condition as given by a point on its component performance map. A representative compressor performance map is presented in Fig. 1. The compressor total pressure ratio is plotted versus inlet corrected airflow rate for selected rotor speeds. The actual compressor operating point is a function of several variables, including mass flow rate of air, compressor efficiency, compressor pressure ratio, and rotor speed. The straight solid line in Fig. 1 represents the compressor operating line at constant throttle passing through the design point; the location of the operating line is determined by the power delivered to the compressor by the turbine. The straight dashed line in Fig. 1 represents the pressure ratio limit attainable for the given corrected rotor speed, i.e., the stability limit. To the right of this line, the compressor operates in a stable manner, and to the left, compressor operation is unstable. This limit is reached when the pressure rise across the compressor produces blade loading levels such that boundary-layer separation is induced over large portions of the blades. In this situation two forms of flow instability can occur, rotating stall and surge; hence, the dashed line is sometimes referred to as the stall or surge line. The distance between the operating line and the stability limit is termed the stall or surge margin or, more generally, the stability margin. Typically, the best engine performance occurs when the compressor is operating near the surge line. This phenomenon occurs because the compressor's highest efficiency and, hence, its design point typically lie near the surge line.

Generally, knowledge of compression system performance is gained through experimentation. However, due to test hardware and economic constraints, only a limited amount of compressor performance and stability data can be obtained. This lack of data is especially apparent for the post-stall regimes, such as surge and rotating stall, because of the detrimental effects these phenomena have on compression and engine systems. In these situations, validated mathematical models can predict performance and stability trends that would be too expensive or difficult to obtain by experimental testing. Furthermore, these models can be used to gain insight into areas that are presently limited by experimental testing, and designers and engineers can investigate cause-and-effect relationships that would otherwise be impractical in ground test facilities. Simulations can be developed for capturing dynamic events such as surge, rotating

stall, and inlet distortion, as well as predicting steady-state performance and transient events such as power excursions (e.g., Refs. 1-5).

The work reported in this report focuses on the development of a three-dimensional (3-D) compression system model for predicting pre-stall compressor performance and potentially post-stall (primarily surge) regimes. It uses semi-actuator disc theory and a stage-by-stage characteristic technique from a one-dimensional (1-D) dynamic compression system model (Ref. 2) and applies it to a 3-D Navier-Stokes flow solver (Ref. 6). Turbomachinery effects of mass bleed, blade forces, and shaft work are modeled as source terms added to the 3-D inviscid Euler equations.

This report is organized such that a brief discussion is first given of other simulation techniques used to predict compressor system performance. Then, the technical approach used in developing the current 3-D model is addressed. This section includes an overview of the 3-D flow solver, NPARC (Ref. 6), and discussion of the 1-D turbomachinery source term modeling technique. Treatment of boundary conditions and the determination of initial conditions are discussed. Next, the implementation of the source term modeling technique into NPARC is presented. This section includes a re-structuring of the existing 1-D compressor code, an estimation of the circumferential force on the fluid due to the compressor blades, and an investigation of the generalization of turbomachinery source distributions from 1-D to 3-D. Overall results and radial profiles of results will be compared with experimental data for uniform inlet conditions. Finally, a summary of conclusions is presented and recommendations for future work are suggested.

2.0 REVIEW OF THE LITERATURE

In efforts to understand the complicated flow environment of gas turbine engine compressors, researchers continue to develop and apply mathematical models through computer simulations. For instance, models have been developed to analyze diminished stability margin due to inlet distortion, unsteady wakes created by a rotating blade row, and complicated 3-D secondary flows generated by rotor and end wall interactions. Prior to describing the current work, previous work in compressor model development is reviewed to obtain an understanding of how the present work compliments and extends previously developed concepts. This discussion focuses on modeling techniques which have been used in attempts to simulate the 3-D phenomena of compression system behavior.

2.1 MODIFIED PARALLEL COMPRESSOR MODELS

Classical parallel compressor theory is characterized by the compression system being divided into circumferential segments or sectors which extend axially through the compressor as shown in Fig. 2. Each segment is assumed to act as an individual compressor with no interaction between segments. All segments share the same stage performance curves and exit to the same boundary condition, usually uniform static pressure. At the inlet boundary, different magnitudes of total pressure and/or total temperature can be specified on each segment and when any one segment becomes unstable, or stalls, the entire compressor is considered unstable or stalled. One

disadvantage of classical parallel compressor theory is the absence of mass and momentum transfer between segments.

Hale and Davis (Ref. 2) developed a 1-D axial compressor code, based on 1-D fluid mechanics for modeling generic compression systems. A stage-by-stage characteristic technique was used to calculate turbomachinery source terms for simulating the effects of compressor blades. These source terms consisted of mass bleed, axial blade force, shaft work, and energy losses associated with the bleed. The Hale and Davis simulation used classical parallel compressor theory in an attempt to model the 3-D nature of inlet distortion. The source term modeling approach used by Hale and Davis is the technique used in conjunction with the work presented in this report. Consequently, a more detailed discussion of the source term calculation technique will be given in Section 3.0.

Kimzey (Ref. 7) developed a quasi-three-dimensional model based on parallel compressor theory to study the effects of inlet pressure and temperature distortion. The Kimzey model divided the compressor axially, circumferentially, and radially to form 3-D control volumes. The governing equations were based on three-dimensional, time-dependent conservation of mass, momentum, and energy. Circumferential and radial momentum were modeled by empirical relationships. The radial work redistributions were approximated by modifying the average stage characteristics with profile corrections for characteristic total pressure and total temperature.

Mazzawy (Ref. 8) developed a multiple segment model also based on parallel compressor theory. He divided the blade rows of the compressor axially, and as in classical parallel theory, the performance of each undistorted blade row was modeled with steady-state characteristics; however, he developed separate characteristics that combined the effects of unsteady flow and distortion-induced compressor stage matching for segments with inlet distortion. Furthermore, unlike classical parallel theory which assumes each segment has the same circumferential alignment through the compressor, Mazzawy circumferentially shifted the segments as they passed through the compressor in order to account for flow angularity (Fig. 3). This model showed significant improvement over the classical parallel compressor theory in the prediction of compressor operability, distortion attenuation through the compressor, and stall margin loss. Mazzawy also developed another model similar to the one described above except it used overall compressor performance characteristics rather than blade-row characteristics. It also provided upstream flow redistribution, circumferential particle swirl, and approximate correlations for unsteady flow effects.

Shahrokhi (Ref. 9) constructed a simulation which more accurately represented the 3-D character of compressor flow by refining classical parallel compressor theory. He used algebraic expressions, in the same manner as Kimzey, to model radial and circumferential mass redistribution as well as work redistribution in a stage-by-stage representation of the compressor. The radial mass redistribution was based on the radial momentum equation and permitted mass transport between adjacent radial segments of the compressor. The circumferential mass redistribution was based on an orifice flow analogy and allowed mass transport between adjacent circumferential segments within the compressor. The work redistribution used scale factors which allowed the stage characteristics to be defined as a function of radius. The radial

redistributions used by this model did not address the complex radial flows present in the compressor.

2.2 MULTI-DIMENSIONAL MODELS

Many multi-dimensional compressor models are based on semi-actuator disc theory. Source term techniques for modeling turbomachinery use semi-actuator disc theory. Semi-actuator disc theory is used to simulate a compressor by replacing blade geometry with an externally imposed discontinuity in flow properties over the axial spacing of the bladed region (Fig. 4). This discontinuity also induces discontinuities in one or more of the conservative properties of the flow field. The greatest advantage of semi-actuator disc theory is the simplification of flow-field geometry that can often be achieved. Semi-actuator disc simulations can easily be executed on workstations or even personal computers and achieve accurate results in a timely manner.

Lindau (Ref. 10) extended a 1-D modeling technique for application in a 2-D, axial-radial, and axial-circumferential dynamic compressor simulation to model the splitter plane of a turbofan engine. He used a flux-difference splitting technique to solve the discretized Euler equations with turbomachinery source terms included in the blade rows. The source terms were computed from experimental information obtainable from 1-D compressor maps and then radially distributed using an algebraic method. Lindau used his model to analytically investigate test cases involving surge and rotating stall. No experimental data were available for comparison. Consequently, the accuracy of his radial redistribution method remains unproven.

Escuret and Garnier (Ref. 11) developed a 2-D, unsteady compressible through-flow computer code which solves the circumferentially averaged Euler equations through blade rows. The blade forces were calculated using steady-state blade row characteristics expressed in the form of relative blade angle, pressure loss coefficient, and Mach number. A time-lag was applied to the blade turning and pressure losses. The blade row model was written in absolute variables but in the reference frame associated with the blading so that the mesh used to compute flow in the rotor blade rows is actually rotating. However, the Euler flow equations for the blade-free volumes were solved in the laboratory or absolute reference frame. The blade row model was incapable of handling reversed flows. This through-flow model was coupled with an unsteady Euler solution for blade-free volumes to create a 3-D compressor code with rotating blade rows.

Tan (Ref. 12) developed a 3-D compressor model using the time-dependent, incompressible Euler equations and semi-actuator disc theory. Each blade row was modeled by a distribution of body forces. These forces were calculated by assuming: (1) the flow field to be locally axisymmetric at each circumferential location, and (2) the flow field to be consistent with the 3-D flow field before and after the blade row. Tan asserted that secondary flow, which is highly three-dimensional, reveals itself in the form of twisted stream surfaces. These stream surfaces can be accounted for by correlations based on classical secondary flow theory and then superimposed on the blade body force calculations.

A three-dimensional, compressible, unsteady, non-uniform axial compressor model using semi-actuator disc theory for simulating both fixed and rotating blade rows was developed by Billet, et. al. (Refs. 13 and 14). In order to include viscous effects in bladed regions, the Navier-

Stokes equations were integrated over a stream tube passing through a single blade section bounded by blade row inlet and exit in the axial direction, initial stream surfaces in the radial direction, and adjacent blades in the azimuth direction. The stream surfaces were obtained from a streamline curvature code. All regions outside of blade rows were modeled as inviscid, allowing the Euler equations to be solved over the blade-free domain by a time-splitting finite difference technique. Because resolution of the 3-D viscous flow field through the blade was computationally expensive, the grids for bladed regions were restricted to blade row inlet and exit, thus eliminating much of the detail of the flow field. Due to this lack of information in the blade rows, empirical information, such as total pressure loss coefficient and relative outlet angle, was required for solution.

Other three-dimensional compression system models have been devoted to resolving the flow around blades. In these simulations, the blades themselves are modeled with the inclusion of viscous effects. The mixing-plane, average-passage, and time-resolved simulations are examples of the types of models being developed (Refs. 15-19). These 3-D models have primarily been used for cascade analysis and rotor/stator design. However, direct application of many of these modeling techniques to modeling compressor stability is impractical due to large computer memory requirements and extensive execution times. For instance, problems typical of the compressor studied in this report might require a week of execution time on a large mainframe computer such as an Alliant FX80 (Refs. 15 and 16).

2.3 PRESENT INVESTIGATION

The author concludes from this brief review of currently available computational models that there is a need for a better state-of-the-art model to investigate three-dimensional flows in compression systems. The following model limitations were noted:

- Uniform exit boundary condition
- Absence or simplicity of radial and circumferential flow redistribution
- Incompressible flow
- Time-independent turbomachinery source calculations
- Computer memory restrictions
- Extended time to reach problem solution

As an effect of flow redistribution caused by the compressor, circumferentially non-uniform swirling flows occur in compressors once the flow has passed through one or more blade rows (Ref. 20). These combinations of strong swirl and non-uniformities induce 3-D effects that are difficult to model in 1-D or lumped component computer simulations. Classical and modified parallel compressor models provide inadequate representation of complex radial and circumferential crossflows present in the compressor. Two-dimensional models fail to

sufficiently reproduce the 3-D flow effects of swirling, non-uniform compressor flow. Some 3-D models are limited to low-speed, or incompressible flows. Other models calculate the effects of turbomachinery only once, independent of time. Many 3-D models are also limited by computational expense; computer memory requirements and computational time reduce the efficiency of these models.

The following sections discuss a new computationally efficient, 3-D simulation technique developed by the author for predicting the pre-stall behavior of gas turbine engine compression systems without expensive computational requirements. The simulation can be executed on a personal computer and a solution obtained in a matter of minutes or hours rather than weeks or months. This simulation is not limited to low-speed compressor flows because it solves the compressible form of the Euler equations. Furthermore, the effects of turbomachinery, modeled as source terms, are updated at every iteration of the solution procedure. This model also possesses the potential to be used for inlet distortion analysis or extended to include post-stall capabilities.

3.0 OVERALL APPROACH

The overall approach taken for the development of this 3-D compression system model is conceptually presented in Fig. 5. NPARC (Ref. 6) is a 3-D time-dependent flow solver for simulating phenomena such as flows through ducts and around airfoils. The NPARC 3-D flow solver was combined with a stage-by-stage characteristics technique for calculating turbomachinery source terms to produce a 3-D compression system model. The following sections discuss the flow solver chosen for this work and the source term modeling technique that was used. Implementation of the source term modeling technique into the 3-D flow solver will be discussed in Section 4.0.

3.1 THREE-DIMENSIONAL FLOW SOLVER (INTEGRATOR)

Because of its power and versatility as a flow solver, NPARC was chosen for this research. NPARC is a three-dimensional, time-dependent, general purpose Navier-Stokes flow solver developed at Arnold Engineering Development Center (AEDC) and NASA Lewis Research Center. It is an extension of the PARC code (Ref. 21) that was developed for use at the Engine Test Facility (ETF) at AEDC and is based on the numerical algorithm implementation developed by Pulliam and Steger (Refs. 22 and 23). The numerical algorithm implemented is a variation of the Beam and Warming implicit approximate factorization algorithm (Ref. 24) applied to the compressible Navier-Stokes equations expressed in curvilinear coordinates. Artificial dissipation terms are explicitly added to the discretized Navier-Stokes equations for numerical stability during computation of early transients and while approaching steady state. The resulting algorithm is very general and has the characteristics of global conservation and shock capturing. NPARC retains the ADI (alternating-direction implicit) style formulation developed by Pulliam (Ref. 23) for more efficient execution times in comparison to other implicit and explicit formulations.

NPARC calculates the thermodynamic and kinematic properties of a compressible fluid flow at discrete points within the flow field for specified boundary flow conditions and geometry.

Problems involving complex geometries can be analyzed, and viscous and inviscid flow fields can be simulated. In addition, steady-state and transient flows can be simulated. NPARC has been used to analyze many propulsion-related problems, including thrust-reversing engine exhaust collector design, free-jet test design for icing studies, study of test cell heating due to diffuser/engine interaction, and diffuser operation (Refs. 25-29).

3.1.1 Governing Equations

The governing partial differential equations in NPARC are the Reynolds-averaged Navier-Stokes equations for a thermally and calorically perfect gas. However, the present research is based on the assumption of inviscid flow; therefore, the continuity, momentum, and energy equations are reduced to the Euler equations written in the following non-dimensional, strong conservation form:

$$\frac{\partial \mathbf{Q}}{\partial t}+\frac{\partial \mathbf{E}}{\partial x}+\frac{\partial \mathbf{F}}{\partial y}+\frac{\partial \mathbf{G}}{\partial z}=\mathbf{S} \tag{1}$$

where

$$\mathbf{Q}=\begin{Bmatrix}\rho\\ \rho u\\ \rho v\\ \rho w\\ \rho e_t\end{Bmatrix};\quad \mathbf{E}=\begin{Bmatrix}\rho u\\ \rho u^2+P\\ \rho uv\\ \rho uw\\ (\rho e_t+P)u\end{Bmatrix};\quad \mathbf{F}=\begin{Bmatrix}\rho v\\ \rho vu\\ \rho v^2+P\\ \rho vw\\ (\rho e_t+P)v\end{Bmatrix};\quad \mathbf{G}=\begin{Bmatrix}\rho w\\ \rho wu\\ \rho wv\\ \rho w^2+P\\ (\rho e_t+P)w\end{Bmatrix};\quad \mathbf{S}=\begin{Bmatrix}S_C\\ S_x\\ S_y\\ S_z\\ S_E\end{Bmatrix}$$

and

$$e_t=e+\frac{1}{2}V^2 \tag{2}$$

Based on the assumption of a thermally and calorically perfect gas, the following non-dimensional equations of state are used:

$$P=\rho T/\gamma \tag{3}$$

$$e=\frac{T}{\gamma(\gamma-1)} \tag{4}$$

which allow pressure and temperature to be expressed as functions of the conservation variables,

$$P = (\gamma - 1)\left(E - \frac{1}{2}\rho V^2\right) \tag{5}$$

$$T = \gamma(\gamma - 1)\left(\frac{E}{\rho} - \frac{1}{2}V^2\right) \tag{6}$$

where

$$E = \rho\left(e + \frac{1}{2}V^2\right) \tag{7}$$

and the ratio of specific heats, γ, is a constant. **S** represents the suitably non-dimensionalized turbomachinery source terms of mass bleed, x-direction force, y-direction force, z-direction force, and shaft work and bleed energy, which are added to the right-hand side of the Euler equations to simulate the effects of compressor blades. The calculation of these terms will be discussed in Section 3.2.

3.1.2 Grid Issues

Before implementing the source term modeling technique into the 3-D flow solver, some issues concerning the grid and its transformation had to be considered. NPARC requires an ordered set of nodal points which symbolizes the geometric boundaries of the flow problem and an appropriate distribution of flow-field points between those boundaries. The physical coordinates are considered Cartesian (x,y,z) and are defined for each integer combination of indices (J,K,L), which represent a curvilinear coordinate system in the computational domain. Generally, right-handed physical and computational coordinate systems are used for all points in the domain. Furthermore, it is important for the grid to vary smoothly with minimal skewness and the boundary and flow gradients to be well resolved in order to obtain the best accuracy and convergence rates. Also, grid spacing near boundaries should be small enough to avoid the introduction of error due to the first-order boundary conditions.

In order to allow for easy discretization on arbitrary grids, the Cartesian form of the Navier-Stokes equations are transformed to a computational domain where the grid spacing is uniform and the domain is rectangular (refer to Fig. 6). The equations are re-expressed in a general curvilinear coordinate system by the following coordinate transformation:

$$\begin{aligned} \xi &= \xi(t,x,y,z) \\ \eta &= \eta(t,x,y,z) \\ \zeta &= \zeta(t,x,y,z) \\ \tau &= t \end{aligned} \tag{8}$$

The NPARC formulation assumes that the curvilinear coordinates do not vary with time.

3.1.3 Boundary Conditions

NPARC has numerous boundary conditions available to its users, but only the boundary conditions used in this research will be considered here. The boundary conditions are denoted (contiguous, slip wall, subsonic inlet, exit) and are applied on the computational domain as shown in Fig. 7. All of the boundary conditions are explicit and first-order accurate. The remainder of this section discusses each boundary condition in detail.

A contiguous, or wrap-around, boundary condition is applied at the circumferential boundary. This boundary condition requires overlapping grid points which match exactly. In all cases considered in this report, the grid overlaps by exactly one cell. Referring to Fig. 7a, values of all conservation variables (ρ, ρu, ρv, ρw, ρe_t) at L_{max}-1 equal those at node 1, and all values at L_{max} equal those at node 2; i.e., this boundary condition is rotationally periodic.

A slip wall boundary condition is used for the compressor walls. Normal velocity components are zero for all solid boundaries, i.e., $\vec{V} \cdot \vec{n} = 0$, and all flow gradients normal to the boundary are zero. Density, pressure, and tangential velocity are extrapolated from points adjacent to the boundary. The slip wall boundary condition is based on the assumption of inviscid flow throughout the computational domain, including at the wall.

The inlet to the compressor provides the inflow boundary. Flow is subsonic at the inlet and assumed normal to the boundary. Total pressure, P_t, and total temperature, T_t, are specified on this boundary. The inflow boundary condition, which is based on reference plane characteristics, uses the compatibility equation constructed along the (u-a) characteristic to pass information from the interior algorithm to the boundary condition. The definitions of total pressure and total temperature along with the compatibility equation are solved iteratively for velocity, static temperature, and static pressure. The conservation variables (ρ, ρu, ρv, ρw, ρe_t) are calculated from the primitive variables (ρ, u, v, w, and P).

The exit of the compressor provides the outflow boundary. The flow is subsonic. The conservation variables are transformed to the primitive variables as in the inflow boundary condition. The static pressure is prescribed at a single grid point at the exit. NPARC adjusts the variation of static pressure at the exit to match the static pressure variation found one grid plane upstream of the boundary. The density and velocity are extrapolated from one grid plane upstream of the boundary. The conservation variables are updated using these values. This boundary condition adequately ensures global continuity.

3.1.4 Initial Conditions

In order to use NPARC as the solver for the simulation, a grid and an initial flow field in the form of a set of conservation variables are required. Although grid requirements are less stringent for inviscid simulations (like the ones presented here) than for viscous simulations, the 3-D grid used for a given problem can still greatly influence the quality and convergence rates of an NPARC solution. The grid concerns addressed in Section 3.1.2 were considered. Grid spacing near boundaries was of particular concern to ensure the first-order accurate boundary conditions were well resolved. A simple method for producing a 3-D grid was found by constructing an

were well resolved. A simple method for producing a 3-D grid was found by constructing an axisymmetric grid using a grid generation package and then spinning the grid about the x-axis for a chosen compressor geometry. An overlap by one grid cell was used in the circumferential direction due to the overlap boundary condition. The locations of all blade rows were identified and in fixed positions. An axial-radial view of a grid used is shown in Fig. 8, and a full three-dimensional grid is illustrated in Fig. 9. The grid was based on an actual geometry for a compressor with a single rotor blade.

3.2 STAGE CHARACTERISTIC METHODOLOGY FOR MODELING TURBOMACHINERY SOURCES

The one-dimensional stage-by-stage characteristic technique used in the development of this 3-D compressor code is based on that applied in the 1-D turbine engine compressor code, DYNTECC (Ref. 2), which was mentioned in Section 2.1. DYNTECC was developed at the Arnold Engineering Development Center for the stage-by-stage, dynamic analysis of generic, axial compression systems. It uses the stage-by-stage characteristic technique for calculating source terms which model the effects of turbomachinery for these compression systems. These source terms, including mass bleed, axial blade forces, and shaft work, are calculated at the cell-centers on a quasi 1-D grid and added to the right-hand side of the 1-D Euler equations in DYNTECC:

$$\frac{\partial}{\partial t}(\mathbf{BA}) + \frac{\partial}{\partial x}(\mathbf{CA}) = \mathbf{D} \tag{9}$$

where

$$\mathbf{B} = \begin{Bmatrix} \rho \\ \rho U \\ \rho\left(e + \frac{U^2}{2}\right) \end{Bmatrix}; \quad \mathbf{C} = \begin{Bmatrix} \rho U \\ \rho U^2 + P \\ \rho U\left(e + \frac{P}{\rho} + \frac{U^2}{2}\right) \end{Bmatrix}; \quad \mathbf{D} = \begin{Bmatrix} -W_{Bx} \\ F_x \\ Q_x + SW_x - H_{Bx} \end{Bmatrix}$$

W_{Bx} represents mass bleed flow rate distribution across system boundaries other than the inlet and exit. F_x symbolizes the axial-force distribution acting on the control volume due to the blade and compressor casing. Compressor shaft work distribution applied to the control volume, heat transfer rate into the control volume, and enthalpy change associated with bleed flow are given by SW_x, Q_x, and H_{Bx}, respectively. A complete set of compressor stage characteristics must be provided for closure of the governing equations.

The compressor stage characteristics provide pressure and temperature variations for each stage as a function of steady-state airflow in the absolute reference frame. Steady-state stage forces, F_x, and shaft work, SW_x, can be calculated by a control volume analysis using these

pressure and temperature rises and airflow rates. This control volume approach is depicted in Fig. 10. A typical set of steady-state stage characteristics presenting pressure and temperature coefficient versus flow coefficient for lines of constant corrected rotor speed is shown in Fig. 11. The characteristics show three distinct regions of compressor operation: pre-stall, rotating stall, and reversed flow. Blade row performance during normal operation is exhibited by the pre-stall characteristic. Rotating stall and reverse flow are post-stall operating regimes. The rotating stall region is based on a flow-weighted average of a fully developed rotating stall cell, and the pressure and temperature ratios represent average pressure and temperature rise across the stage for both stalled and unstalled flow. The reversed-flow characteristic region represents the pressure loss and temperature rise associated with full-annulus reversed flow. To provide a dynamic characteristic, Hale and Davis (Ref. 2) imposed a first-order time lag on the stage forces for the rotating stall region since the globally steady-state characteristics were not applicable for dynamic events such as transition to surge or development of rotating stall. This time lag equation was

$$\tau \frac{dF_x}{dt} + F_x = (F_x)_{ss} \tag{10}$$

where τ is the time constant used to calibrate the model to provide correct post-stall behavior, F_x is the blade force and pressure-area force, and $(F_x)_{ss}$ is the steady-state blade force and pressure-area force obtained from the steady-state compressor characteristics.

The exact form of the steady-state compressor characteristics can vary, depending on which form lends itself to the most accurate implementation of the characteristics by the simulation and the form of the data which is readily available to the user. To ensure the most accurate reading of the characteristic maps, the form chosen should give the smoothest surface in operational space. The following formulation of the characteristics was chosen for this work, with the stage flow coefficient, Φ, given as

$$\Phi = W'_{cor} \tag{11}$$

where

$$W'_{cor} = \frac{W\sqrt{TR}}{PR} \tag{12}$$

with

$$TR = \frac{T_t}{(T_t)_{ref}} \tag{13}$$

and

$$PR = \frac{P_t}{(P_t)_{ref}} \tag{14}$$

and the pressure coefficient, Ψ^P, and the temperature coefficient, Ψ^T, are given as

$$\Psi^P = (PR - 1) \tag{15}$$

$$\Psi^T = (TR - 1) \tag{16}$$

respectively. Typical plots of Ψ^P and Ψ^T versus Φ are shown in Figs. 11a and b, respectively.

DYNTECC calculates initial conditions based on user-specified flow conditions and the compressor geometry. The boundary condition for the source calculations requires total pressure, total temperature, and corrected mass flow rate at the stage inlet. The exit boundary condition requires the specification of either static pressure, mass flow rate, or Mach number. A discussion of how DYNTECC works is presented in Section 4.1 of the following section.

3.3 THREE-DIMENSIONAL COMPRESSION SYSTEM MODEL

The1-D, stage-by-stage characteristic approach for calculating turbomachinery source terms was combined with the 3-D flow solver, NPARC, to produce a 3-D compression system model. Overall values of total pressure ratio and total temperature ratio are obtained from steady-state stage characteristics. These overall values produce average values for the source terms: axial force, circumferential force, and shaft work, on a per volume basis. These average values are then distributed axially, radially, and circumferentially. This process of implementing the source term calculations into NPARC is discussed in the following section.

4.0 IMPLEMENTATION OF STAGE CHARACTERISTIC TECHNIQUE

This section discusses the implementation of the stage characteristic source term technique into the 3-D flow solver. The source term modeling technique is adapted from the quasi 1-D compressor code, DYNTECC. The DYNTECC one-dimensional technique for modeling turbomachinery effects in the axial direction is applied and extended to the circumferential direction. The axial force, circumferential force, and shaft work computed by the 1-D technique are extended to 3-D for implementation into the three-dimensional solver. Radial characterization of the source terms will be covered in Section 5.0.

4.1 ADAPTATION (RE-STRUCTURING) OF DYNTECC SOURCE CALCULATIONS

To facilitate the addition of the stage characteristic approach for calculating source terms into NPARC, some existing lines of code were extracted from DYNTECC. In order to better understand this process, the structure of DYNTECC is discussed briefly, and then the general modifications necessary to incorporate the existing code into NPARC are presented.

Referring to Fig. 12, DYNTECC is composed of three basic parts: the stacker, the integrator, and the source term calculator. The steady-state stacker initializes the entire quasi 1-D compressor flow field to some initial state as specified by user inputs. Initial conditions for the control volumes are calculated using steady flow physics (general equations of gas dynamics), pre-stall compressor stage characteristics, and user-specified inputs including percent corrected speed, initial airflow rate, and initial steady-state values of total pressure and total temperature. The integrator solves the 1-D Euler equations by a numerical technique. The source term calculator calculates the turbomachinery source terms using the stage characteristic approach, which is of primary interest to this research.

As mentioned above, the source term calculator is of primary interest. Therefore, the integrator was eliminated entirely. Next, the source term calculator was reduced to a single subroutine, so that all communication between NPARC and the source term calculator is controlled by argument list . The source term calculator uses NPARC as its integrator. The only major piece left is the stacker. As mentioned in Section 3.1.4, NPARC requires an initial flow field for the entire compressor in the form of a restart file in order to get started. Therefore, the stacker was incorporated into a routine for calculating a good initial guess of the overall compressor flow field. The stacker is used to generate a quasi 1-D set of initial conditions on the simple 1-D grid used by DYNTECC, e.g., the grid shown in Fig. 13; that is, the stacker initializes the one-dimensional flow field (conservation variables) and sources. The conservation variables are non-dimensionalized by the NPARC standard. An Akima spline (Ref. 30) is used to distribute the non-dimensionalized conservation variables radially from the 1-D grid to the 3-D grid. The resulting axial-radial distribution of conservation variables is spun circumferentially so that all nodes in the computational domain are initialized. The circumferential force (see Section 4.2) is calculated by the stacker so that the effects of swirl are included in the initial conditions. The preceding methodology for generating an initial flow field has the consequence of producing an initial guess which is close to the final 3-D solution produced by NPARC by iteration. This initial guess reduces the number of iterations required for a steady solution and increases the maximum time step that can be used.

4.2 ESTIMATION OF CIRCUMFERENTIAL FORCE

Using the source term methodology of DYNTECC discussed in Section 3.2, turbomachinery effects in the axial direction can be simulated. Following this source term modeling approach, the force in the circumferential direction produced by swirl can also be calculated. Compressors do work on a fluid by increasing the angular momentum of the fluid stream, which effects the tangential velocity component of the flow. The Euler turbomachinery equation relates the changes in angular momentum to power input as given by

$$\mathcal{P} = W\,\omega\left(r_e v_e' - r_i v_i'\right) \tag{17}$$

where W is the mass flow, ω is the rotor rotational speed, v_e' and v_i' are the exit and inlet tangential velocities, respectively, and r_e and r_i are average radii at the inlet and exit of the blade row, respectively. Compressor power written in terms of the torque is

$$\mathcal{P} = \Gamma \omega \tag{18}$$

Equating the above equations and recalling that torque can be defined as a force acting through, in this case, a mean radial distance, the following relationship can be derived:

$$F_\theta = \frac{W}{r_{avg}} \left(r_e v'_e - r_i v'_i \right) \tag{19}$$

where F_θ is the average circumferential force, and r_{avg} is an average radius over the entire blade row. This equation permits the average circumferential force produced by swirl to be estimated. The total energy of the compressor remains constant but the axial momentum decreases to account for the tangential component. This approach allows for the inclusion of swirl in a one-dimensional, axial simulation. The accuracy of this average circumferential force is determined by the accuracy of the average radius used.

4.3 TURBOMACHINERY SOURCE DISTRIBUTIONS

The one-dimensional source term modeling technique discussed in Section 3.2 was adapted for inclusion in NPARC as discussed above in order to simulate the three-dimensional effects of turbomachinery. Mass bleed, axial blade/casing forces, circumferential forces, and shaft work are modeled as source terms added to the right-hand side of the Euler equations [Eq. (1)]. As in the 1-D technique, the axial forces and shaft work are calculated from a set of one-dimensional, steady-state stage characteristics based on experimental data. The circumferential force is calculated based on the Euler turbomachinery equation (see Section 4.2). All source terms are known on a per volume basis, rather than a per length basis as in DYNTECC, at the center of each cell in a bladed region. The per volume basis is necessary due to the 3-D nature of NPARC. The stage characteristic approach uses a simple 1-D grid with vertical grid lines, as depicted in Fig. 13, on which to calculate the source terms; NPARC uses a 3-D grid which is generally much more complex and, in physical space, may or may not have vertical grid lines. Additionally, in NPARC, all properties are known on cell nodes rather than cell centers; therefore, a method for specifying the source terms on the nodes and distributing them throughout the 3-D grid of each blade row was developed. The following discussion describes the entire source term calculation process as it applies to the 3-D code. This process is illustrated by the flow chart in Fig. 14.

Each blade row of the compressor is modeled using semi-actuator disc theory. A set of axial indices relating the bladed regions to the overall geometry for multiple blade rows was developed to facilitate the specification of sources within the blades for each blade row. Once the blade indices have been computed for all blade rows, DYNTECC's stacker (refer to Section 4.1) is used to initialize conditions for the turbomachinery calculations for the first NPARC iteration. For subsequent iterations, the source calculator computes one set of sources (four values: one bleed, one axial force, one circumferential force, one shaft work) for each blade row on the simple, one-dimensional grid.

As stated earlier, to calculate the forces and shaft work terms for the momentum and energy equations, the mass flow rate, total pressure, and total temperature at the inlet to the blade

row must be known. To compute these local properties, the NPARC flow field is sampled at the inlet to each blade row for each circumferential segment. Average values of total pressure and total temperature are calculated from the local conservation variables at these points, and total pressure, total temperature, and mass flow rate are dimensionalized to a consistent set of units. The sum of the local radial mass flow rates at the blade inlet gives the mass flow for one circumferential segment. The overall compressor mass flow rate is the sum of the mass flows for each circumferential segment. Given the computed local values for total pressure, total temperature, and overall mass flow, the turbomachinery sources are calculated using the technique described in Section 3.2.

Due to the non-dimensional formulation of the equations for the NPARC solver, after the 1-D sources are calculated, they must be non-dimensionalized. The following non-dimensionalizations were used:

$$
\begin{aligned}
S_C &= \frac{W_B}{\rho_{ref} a_{ref}} \\
S_x &= \frac{F_x}{\rho_{ref} a_{ref}^2} \\
S_y &= \frac{F_y}{\rho_{ref} a_{ref}^2} \\
S_z &= \frac{F_z}{\rho_{ref} a_{ref}^2} \\
S_E &= \frac{SW + H_B}{\rho_{ref} a_{ref}^3}
\end{aligned}
\tag{20}
$$

where

$$
\begin{aligned}
\rho_{ref} &= \frac{P_{ref}}{RT_{ref}} \\
a_{ref} &= \sqrt{\gamma RT_{ref}}
\end{aligned}
\tag{21}
$$

and

$$
\begin{aligned}
F_y &= \left(F_r \cos\theta_L - F_\theta \sin\theta_L\right) \\
F_z &= \left(F_r \sin\theta_L + F_\theta \cos\theta_L\right)
\end{aligned}
\tag{22}
$$

S_C is mass bleed flow rate, S_x is the x-direction or axial force, S_y is the y-direction force, S_z is the z-direction force, and S_E is the shaft work and any bleed enthalpy. P_{ref}, T_{ref}, ρ_{ref}, and a_{ref} are reference quantities and R is the gas constant for air. Equation (22) is the trigonometric

relationship that transforms the circumferential force, F_θ, and the radial force, F_r (which is assumed to be zero), to the appropriate circumferential segment in Cartesian coordinates. A derivation of the appropriate non-dimensionalizing parameters for the sources is given in Appendix A. Furthermore, the sources are on a per volume basis and must be divided by the local, node-centered Jacobian (1/ computational cell volume) of the transformation to computational space before being added into the solver to be consistent with the numerical scheme before the new sources were added. Finally, the non-dimensionalized, 1-D sources must be distributed to the nodes of the 3-D grid.

4.3.1 Axial Distribution of Source Terms

A weighting distribution procedure is used to compute a weighting function for distributing the sources in the axial direction, in the blade row, and on the 3-D grid, because the bladed region represents a blade with a finite axial span. This weighting algorithm allows the user to specify a distribution shape. The shape is defined by integer values assigned to blade row inlet and exit, an integer value for a midpoint within the blade row, and a percentage of dwell on either side of the midpoint. The integer values range from zero to eight, with zero having no source assigned to that node and eight having the full magnitude of source assigned to that node; this allows the user to linearly ramp the amount of source present axially through the blade row. The percentage of dwell at the midpoint allows the user to specify a constant value over a given range of nodes within the blade row. An illustration of one distribution is shown in Fig. 15a. The range of integer values was randomly chosen; another range, say one to ten, could be used.

The weighting function is calculated from local volumes in the blade row and the specified distribution function. A radial distribution of weighting functions is produced because the volume varies for each axial slice through the blade. The weighting function is calculated by

$$\lambda_{jk} = \delta_k d_j \tag{23}$$

where the radial distribution, δ_k, is given by

$$\delta_k = \frac{\forall_k}{\left(\sum_j d_j \forall_j\right)_k} \tag{24}$$

and d_j is the distribution function. $\forall_k$ is the sum of the local volumes, $\forall_j$, in an axial slice. The result is a conservative radial distribution of weighting functions which is applied in the axial direction through each blade row. Figure 15a shows one possible distribution shape. This shape denotes that the sources are ramped from zero to maximum values and held at these maximum values through the middle of the blade. The sources are then ramped back down to zero at the exit of the blade row. This shape has the effect of bringing on the sources gradually in the axial direction in an attempt to circumvent convergence problems due to a sudden discontinuity in flow caused by the sources. The distribution shape shown in Fig. 15a was used with a good

degree of performance, but it was later discovered that the simple uniform axial distribution shown in Fig. 15b was better from a numerical stability standpoint because the uniform axial distribution produced slightly better convergence rates. The shape in Fig. 15b represents sources that are evenly distributed, i.e., every node contains the same values of sources. Accuracy was unaffected by the axial distribution chosen. Convergence rates were influenced by the axial distribution. The axial source distribution needed might have been deduced from the wall static pressure distribution in the axial direction in the rotor plane, if that information had been available. Since this type of experimental data was not available, the axial distribution of sources was based on the robustness of the solution technique.

4.3.2 Circumferential Distribution of Source Terms

Two methods were used to distribute the sources in the circumferential direction. The simplest way was to develop the radial distribution and then spin the result of this axial-radial distribution circumferentially so that all nodes in the 3-D grid of the blade row contained a set of sources; this procedure was repeated each iteration to update the source terms. This was the method of choice. Another method was to calculate the sources for each circumferential segment. This method required the stage characteristic source term calculator to be called for every circumferential segment for every iteration, and thus required slightly longer execution times. However, for cases involving non-uniform inlet conditions, such as inlet distortion, the latter method would be appropriate and necessary for obtaining accurate solutions.

5.0 INVESTIGATION OF THE RADIAL CHARACTER OF SOURCE TERMS

Developing an approach to distribute the sources radially required an investigation of the radial character of source terms using a test case. A simple uniform radial profile of sources was used and found to be inadequate, as discussed in the following sections. Due to the inaccuracy of the results of this method, a streamline curvature code (Ref. 31) was used to investigate the radial character of the sources. The knowledge gained from this investigation led to two other methods of distributing the sources radially. This section discusses these three methods of radially distributing the source terms. First, a brief description of the test case, including grid development, is presented. Then, the validity of the stage characteristic approach for calculating the source terms is considered. Next, the results using uniform radial profiles of source terms is compared to experimental data. Results using the two methods developed from the streamline curvature code investigation are also compared to experimental data. All data comparisons are made in the absolute reference frame. Finally, the effects of grid resolution on the accuracy of the results are briefly discussed.

5.1 EXPERIMENTAL COMPRESSION SYSTEM, ROTOR 1B

An axial-flow compressor consisting of a single-stage, high-speed rotor was used as the test vehicle for this research. This rotor, referred to as Rotor 1B (Ref. 32), was tested by the National Aeronautics and Space Administration (NASA) in 1967. The rotor had a transonic tip speed of 1400 ft/s, a tip radius of 18.25 in., and a hub-tip radius ratio of 0.5 at the rotor inlet. The rotor was comprised of 44 blades with double-circular-arc blade sections and a mid-span damper. The rotor was designed to have a total pressure ratio of 1.60 and an efficiency of 0.858 at a corrected

flow rate of 215.49 lbm/sec at 100-percent corrected rotor speed. Both overall performance and blade-element data for uniform inlet flow at four different speeds (50-, 70-, 90-, 100-percent corrected speeds) were available for comparison. A total pressure ratio of 1.638 and an efficiency of 0.895 were actually attained.

The grid developed to represent Rotor 1B is shown in Fig. 8. The blade location is noted, as are two reference points. These two reference points denote the location of instrumentation used in the compressor rig test performed by NASA; all data taken at these reference points were adjusted during the experimental data reduction process to obtain conditions at the blade edges. Grid packing was used within the blade row and in the area surrounding the blade. This grid was comprised of 69 axial points, 13 radial points, and 26 circumferential points. A study was conducted to determine if the flow field solutions were unaffected by further refinement of the grid (grid convergence). This study is discussed in Section 5.6.

All experimental data used for comparisons with the model were obtained from Ref. 32. The uncertainty of this data is not discussed in the reference. The methods of obtaining the pressure and temperature measurements, however, are identified as pressure probes and thermocouples, respectively. Although it is impossible to definitively conclude the uncertainty of the data from this information, it is expected the uncertainty should be approximately the same as for other reported pressure and temperature measurements from similar instruments. A review of Ref. 33 indicates that the uncertainty in the pressure measurements can range from ± 0.0175 to ± 0.5 psia, and the uncertainty in the temperature measurements can range from ± (0.38 percent reading + 2°R) to ± (0.75 percent reading + 4°R).

5.2 VERIFICATION OF STAGE CHARACTERISTIC APPROACH

Before applying the 3-D model to simulate Rotor 1B, the stage characteristic technique was verified as an adequate representation of overall performance for Rotor 1B. To accomplish the verification, the 1-D DYNTECC model, from which the source term technique was adapted, was configured for Rotor 1B. Then, DYNTECC was run for several points at four corrected speeds and its results compared to the experimental overall performance map. This comparison is shown in Fig. 16. The stage characteristic technique was able to reproduce the overall performance of the rotor. As a result, it was assumed the technique was valid, i.e., the stage characteristics were constructed correctly and accurately read by the simulation, and the 3-D model could then be tested. The line connecting the four speed lines is the compressor operating line at constant throttle, giving 15-percent stall margin at 100-percent speed. This line was determined experimentally by NASA and will be referred to as the constant throttle line. All subsequent comparisons with experimental data will be made at the intersection of this line with each of the four speed lines.

5.3 UNIFORM RADIAL DISTRIBUTION OF SOURCES

In order to test the new 3-D model using the stage characteristic approach, the model had to be configured for the test case and a radial distribution of the source terms had to be assumed. Initially, a uniform radial distribution of turbomachinery sources was assumed. The uniform method applies the calculated 1-D sources equally to each radial node; i.e., each of the three 1-D

sources produces a uniform (slug) profile as depicted by Fig. 17. This same type of profile would be predicted by parallel compressor theory under uniform inlet flow conditions. The model was then executed for four points along the compressor operating line at constant throttle giving 15-percent stall margin at 100-percent corrected speed (henceforth this line will be referred to as the constant throttle line). The overall results using this simple methodology are compared to experimental data in Fig. 18. The results compare very well to the experimental overall compressor performance map. However, radial comparisons of the flow field tell a different story.

Numerical and experimental data at a point on the constant throttle line for 50-percent corrected speed are compared in Figs. 19 and 20. Figure 19a compares a radial distribution of total pressure ratio to experimental data. Figure 19b shows a comparison of total temperature ratio. Radial profiles of both of these parameters are within 1 percent of that obtained experimentally. Other flow parameters, including absolute exit Mach number, absolute exit velocity, static temperature, and static pressure, were within 7 percent of that obtained experimentally; absolute exit velocity and exit static pressure are plotted in Figs. 20a and b, respectively, as typical examples. Radial profiles of flow parameters, and thus any ratios formed from these parameters, are products of the swirl produced by the blades (which is simulated by the circumferential force). Figure 21 is representative of typical swirl velocities produced by the compressor.

As speed was increased, the uniform radial source profiles (shapes, not magnitudes) did not perform as well as they did at 50-percent speed. Total pressure ratio and total temperature ratio at the constant throttle line point for 100-percent speed are compared with experimental results in Figs. 22a and b, respectively. Total pressure ratio is within 13 percent of experimental data, and the difference in total temperature ratio has increased to over 2 percent. The maximum difference among other flow parameters was large, almost 20 percent, as exhibited in the plots in Fig. 23. The uniform profiles missed some of the physics associated with the hub and tip regions of the rotor. Therefore, radial redistributions of the sources were studied in attempts to model the effects around the hub and tip more appropriately.

5.4 RADIAL REDISTRIBUTION IMPLEMENTATION

Radial redistribution could be applied to the total pressure and total temperature ratios. However, the configuration of the stage characteristic technique lends itself more easily to radial redistribution of the turbomachinery source terms. In order to determine the radial character of the source terms, a streamline curvature code (Ref. 31) was used to predict the compressor performance. This code, called CPAC, is based on radial redistribution of turbomachinery source terms (blade forces and shaft work) for axisymmetric flow. It assumes that entropy and enthalpy do not change along streamlines except as prescribed by loss and deviation across the blades. Again, the purpose of using the streamline curvature code was to determine appropriate radial redistributions of source terms. Radial redistribution of sources (axial and circumferential forces and shaft work) was less complicated than radial redistribution of pressure and temperature. If pressure and temperature were used, additional calculations would need to be made since the modeling technique uses sources as inputs.

The streamline curvature code had previously been tailored by Hale (Ref. 34) for the test case Rotor 1B. The code used the exact losses and deviations from the experimental results, rather than correlations, to calculate the source terms and resulting flow field. A comparison of the overall performance calculated from the code and the experimental results is presented in Fig. 24. Radial performance at two points along the constant throttle line (giving 15-percent stall margin at design speed) is also compared. A comparison at 50-percent speed is shown in Fig. 25. Another comparison at 100-percent speed is shown in Fig. 26. As can be seen in these figures, the streamline curvature code accurately reproduces both overall and radial performance. Consequently, the code was assumed to be an accurate method of predicting the radial character of the turbomachinery source terms. Since CPAC proved to be an accurate method of reproducing radial performance using source terms, the source terms that were calculated during the verification process above were compared in order to determine a correlation, if possible. The following section discusses the development of two correlations from knowledge gained using the streamline curvature code.

5.5 RADIAL REDISTRIBUTION CORRELATIONS

In order to develop correlations for radial redistribution of source terms, the radial profiles of all the sources calculated by the streamline curvature code were compiled. Since the present modeling technique contained no mechanism for calculating a radial force, all radial forces, being at least one order-of-magnitude smaller than the axial force, circumferential force, and shaft work, were ignored. The sum of the radial sources per volume multiplied by their respective elemental volumes was calculated and the result divided by the total volume of the blade row. Then, each radial distribution was normalized by this average source per volume. Finally, the sources per volume were compared in two different ways. The following two sections describe this process and the results as compared to experimental data. Section 5.5.1 describes a correlation based on speed, and Section 5.5.2 describes a simple correlation based on mass flow.

5.5.1 Radial Distribution Based on Collapse in Speed

The correlation based on speed found from the investigation using the streamline curvature code was discovered by plotting each normalized source versus normalized mass flow at different radial locations. The difference in mass flow from the mass flow rate at stall along each speed line was normalized by the change in mass flow rate from choke to stall for that speed. Figure 27a shows normalized shaft work per volume versus normalized mass flow at the hub, mean, and tip for all four speeds. Normalized shaft work per volume is illustrated in the figure, but the profiles shown are typical for axial and circumferential forces per volume, as demonstrated in Figs. 27b and c. As indicated in the figure, the profiles are similar for all speeds at a given radius, especially for the mean radius. Furthermore, a fairly strong distribution can be seen from hub to tip.

Since the sources appear to collapse well in speed at different radii, a correlation was developed to produce radial profiles of sources based on this observation. First, a mean curve was drawn through the normalized source plots in Fig. 27 as depicted by the solid line, and the same procedure was applied at all other radii. Next, since the profiles shown were typical of all the sources, only one set of curves was chosen, i.e., the shaft work curve for each radius. A shift

factor was applied to the set of shaft work curves to reproduce the curves for the circumferential force. This was necessary because the shape of the circumferential force profiles was similar to that of the axial force and shaft work but the magnitudes were different. Finally, an interpolation routine was developed to generate the correct profile based on the corrected mass flow.

The technique described above was implemented into the 3-D model, and the model was run for four points along the same constant throttle line used previously. The overall performance along the constant throttle line predicted using this radial redistribution is shown in Fig. 28. As can be seen in the figure, the model predicted the overall performance, as did the uniform distribution, within 1 percent of that obtained experimentally. However, an improvement in the radial prediction of the flow field over that computed using the uniform distribution is indicated. Figures 29a and b compare numerical and experimental results for total pressure ratio and total temperature ratio, respectively, at the point lying on the constant throttle line for 50-percent speed (same point used for comparison using uniform radial source profiles). As with the uniform radial distribution, total pressure ratio and total temperature ratio were within about 1 percent of the experimental data. Most other flow parameters were within 6 percent of that demonstrated experimentally, as shown in Fig. 30. The same trend was observed for these radial profiles as for the uniform profiles; i.e., as speed increases, flow field differences increase. However, in general, the performance is better than that which resulted from using the uniform profiles.

Another comparison of the constant throttle line point at 100-percent speed is presented in Fig. 31. Careful examination of Fig. 31a reveals that the difference in total pressure ratio actually increased over that resulting from the uniform radial profiles, e.g., 12.5 percent to 28 percent, but the difference in total temperature ratio (Fig. 31b) decreased to about 1 percent. As a result of the poorer performance for 100-percent speed, the maximum difference using this method of distributing the sources radially was approximately 30 percent, as exhibited by the absolute exit velocity in Fig. 32. The large differences exhibited at 100-percent speed could be attributed to a weak correlation at that speed. Referring back to Fig. 27, the correlation does not match the shape for 100-percent speed as well as it did for the 50-percent speed, especially at the hub. Consequently, another approach for radially distributing the sources was considered.

5.5.2 Radial Distribution Based on Collapse in Mass Flow

The second correlation gained from the streamline curvature code investigation was discovered by plotting normalized sources per volume versus radius for different mass flows. Figure 33 shows normalized axial force, normalized shaft work, and normalized circumferential force, all on a per volume basis, versus radius. The clockwise-directed arrows denote the increase in mass flow, pivoting about the mean line. These plots are typical for all speeds. Again, the magnitude of the normalized sources varies greatly from hub to tip. However, the shape of the source profiles remains similar for all mass flows.

The above observations led to a simple linear correlation based on a collapse in mass flow for each source. A mean curve was drawn through the plots in Fig. 33 as depicted by the dotted line. Then, a line was drawn through each of the three curves as approximated by the solid line on the right in Fig. 33. This resulted in three linear profiles, one for each of the forces and shaft

work. The three linear profiles were held constant, regardless of the corrected speed or mass flow.

This simple linear redistribution was implemented into the 3-D model in such a way that the overall source distribution was equivalent to that obtained from a slug distribution, and again, the model was run for four points along the constant throttle line. The results using this simple method were improved over the slug distributions and the correlation based on speed. The model accurately predicted the overall compressor performance along the constant throttle line as illustrated in Fig. 34. Furthermore, an improvement over the previous two methods was exhibited in the radial flow field accuracy. The results at the same two points at 50- and 100-percent corrected speed are compared to experimental data in Figs. 35-36 and Figs. 37-38, respectively. Figure 35a shows the radial distribution of total pressure ratio for the 50-percent speed case, and the difference between this parameter and data is still around 1 percent. The difference in the total temperature ratio shown in Fig. 35b has been reduced to less than 0.5 percent. Figure 36 presents further evidence that this radial distribution might be acceptable. The absolute exit velocity shown in Fig. 36a is within 5.8 percent of the experimental data, and the difference in the exit static pressure of Fig. 36b is less than 1 percent. The maximum difference for most flow parameters was less than 6 percent. An increase in percent difference was still observed as speed was increased, but the difference did not grow as large as in the other two methods of radially distributing the sources.

At 100-percent speed, the total pressure ratio is within 6 percent of that obtained experimentally, as shown in Fig. 37a. This is a 50-percent reduction in the maximum difference for this parameter as compared to the difference calculated using uniform source profiles and a 75-percent reduction over the interpolated profiles based on a collapse in speed. The difference in total temperature ratio (Fig. 37b) was reduced by over 65 percent to within 0.7 percent of the experimental data. A 50-percent reduction in percent difference for most other flow parameters was indicated as exhibited by the absolute exit velocity and exit static pressure in Figs. 38a and b, respectively. Using the linear radial source profiles, the compressor simulation was able to reproduce the compressor performance map as shown in Fig. 39.

A comparison summary of percent differences for some flow field parameters using the three different approaches for specifying the radial source profiles is presented in Table 1.

5.6 GRID REFINEMENT AND OTHER FACTORS

As mentioned in Section 5.1, a study of grid convergence was conducted. Grid convergence typically means that the flow solution is independent of the grid density. Four grids were used to compute results near the design point at 100-percent corrected speed. The base grid was considered to be the grid described in Section 5.1 and illustrated in Figs. 8 and 9. It consisted of 69 nodes axially, 13 radially, and 26 circumferentially, giving it the designation 69×13×26. A second grid approximately doubled the axial dimension, 131x13x26. A third grid approximately doubled the radial dimension, 69×24×26. The last grid approximately doubled the circumferential dimension, 69×13×50. A comparison was made based on total pressure ratio. No notable difference was observed between the base grid and either the 131×13×26 grid or the 69×24×26 grid. An improvement of approximately 0.5 percent was achievable using the

69×13×50 grid. For the present research, this improvement in accuracy was deemed insufficient to warrant the increase in convergence and execution times characteristic of using the circumferentially denser grid.

Other considerations were found to be important for running the model in certain regions of compressor performance. In general, to move to different steady-state operating points on a speed line once a steady-state solution was obtained at an initial operating point, the static pressure specified at a point at the exit was either increased or decreased. In order to run the model in the choked regions of performance (regions where the characteristics are steep), a variable relaxation factor was applied to the source terms; i.e., a different relaxation factor was applied to the sources per volume at each axial station through the blade row. This relaxation factor took the following form:

$$\overline{S} = \overline{S}^{o} + \varphi\left(\overline{S} - \overline{S}^{o}\right) \tag{25}$$

where $\overline{S}$ represents the sources, $\overline{S}^{o}$ is the source values from the previous iteration, and φ is the relaxation factor. A geometric progression was used to vary the relaxation factor through the blade row. The relaxation factor prevented the source terms from moving too far with small changes in mass flow rate. The relaxation factor was predominately applicable at higher speeds, e.g., 90- and 100-percent corrected speeds. A relaxation factor of 0.7 was found to be adequate for obtaining accurate solutions in these regions.

Finally, running the model for regions in which the characteristic was very flat, e.g., 50-percent speed and at points nearing stall at higher speeds, also required special attention. In these regions, small movements of the exit static pressure resulted in large movements in mass flow. Consequently, very small incremental movements of the exit static pressure were required to move to the desired operating point.

6.0 SUMMARY AND CONCLUSIONS

This section presents a summary and discussion of the results from the research conducted for this report. Recommendations and further considerations for future improvements to the model are also discussed. Finally, the implications of this model for surge analysis are presented.

6.1 SUMMARY OF THE RESULTS

The objective of this research was to develop a three-dimensional compression system model using an existing 3-D flow code and a proven 1-D methodology for calculating turbomachinery source terms. The model was assembled, and its ability to predict pre-stall compression system behavior was investigated for a simple compressor consisting of a single rotor. The results are summarized below:

- A quasi 1-D approach for calculating turbomachinery source terms was adapted for the 3-D flow solver, NPARC.
- Pre-stall overall performance was accurately predicted (within 3 percent of data).

- A uniform radial distribution of sources for Rotor 1B produced an inaccurate flow field (20-percent maximum difference compared to data).

- A linear radial distribution of sources reduced the flowfield differences by 50 percent.

- A relaxation factor was used on the source terms in choked regions of compressor performance.

- Grid refinements in the axial and radial directions had no effect on the accuracy of the solutions obtained, but a circumferential grid refinement improved solution accuracy by 0.5 percent.

The following section discusses the results of this investigation in more detail.

6.2 DISCUSSION OF THE RESULTS

The 1-D stage-by-stage characteristic approach for calculating turbomachinery source terms used by DYNTECC was implemented into the 3-D flow solver NPARC. On implementation of the source terms into NPARC, it was discovered that proper distribution of the sources in the radial direction was imperative to achieve accurate flow field results but not so important for predicting the overall performance of the simple test compressor. Three methods for specifying the radial distribution of sources were investigated. Overall, the uniform radial source profiles exhibited the poorest performance, and the linear radial distributions of source terms provided the most accurate flow-field solutions. In all three cases, model predictive accuracy decreased as the corrected speed of the compressor was increased. However, the weighting function applied to the axial distribution of the sources had little effect on model performance. Furthermore, grid density did not seem to be a significant issue for obtaining accurate results. A fairly coarse grid, 69x13x26, with packing within and on either side of the blade, was used with a good degree of accuracy. All solutions were obtained on a 200-MHz P6 PC and required approximately 15 min to reach convergence. Finally, a relaxation factor was necessary to run the model in choked regions of compressor performance.

6.3 RECOMMENDATIONS AND FURTHER CONSIDERATIONS

The integration of a 1-D turbomachinery source term calculation technique and a 3-D flow solver into a three-dimensional compression system model was shown as a viable simulation approach. However, several issues need to be addressed to improve the model and expand its usefulness. A summary of these recommendations is provided below:

- Implement radial re-distribution of source terms for pre-stall compressor performance

- Implement post-stall radial distributions of source terms

- Develop modified boundary conditions for reversed flow conditions and inlet distortion analysis

- Model and implement a simulation of multiple blade rows
- Obtain or develop improved stage characteristics, especially for post-stall operation

The following sections discuss some of these issues in more detail.

6.3.1 Radial Source Redistributions

One important issue for additional consideration is obtaining accurate radial source distributions. One way to improve model performance might be to use a three-point linear radial distribution of source terms. Reviewing the profiles in Fig. 33, the circumferential force is not as well represented by the solid line as it would be using a three-point line pivoting about the mean radius. The shaft work profile would also benefit from this modified linear distribution.

Another idea is to use the streamline curvature code to calculate the source terms instead of using the stage characteristic approach. However, before taking such a drastic step, one must anticipate future applications for this model. A need exists for a compression system simulation capable of analyzing the 3-D flow field during surge cycles. The stage characteristic approach easily affords itself to this type of analysis, and in fact, has been used in 1-D models for surge cycle analysis (Refs. 1, 2, 5). The streamline curvature code, on the other hand, is not a proven methodology in the realm of post-stall analysis. However, perhaps the streamline curvature code methodology could be combined in some manner with the stage characteristic approach to produce accurate radial source profiles while maintaining a post-stall potential.

The radial distribution problem becomes further complicated by the transition to single stage and/or multiple stage turbomachines. The streamline curvature code gave some insight into what the source profiles look like for a single rotor. It might also be useful for investigating source profiles for single and multiple stage compressors.

6.3.2 Post-Stall Radial Source Redistributions

After the settlement of the radial distribution procedure for pre-stall analysis, an assumption must be made regarding the radial distribution mechanism in the post-stall regimes. Since little is known about these profiles during post-stall, one such assumption could be to use the same distribution as was used during pre-stall operation. In the opinion of this writer, this seems to be a logical course of action. Another option would be to use a computational fluid dynamics (CFD) code in reverse flow to provide insight into the above assumption. Also, a methodology for determining and interpreting the onset of stall in a three-dimensional sense needs to be developed.

6.3.3 Boundary Condition Modifications

The inlet and exit boundary conditions in NPARC need to be investigated, and probably modified, for situations involving reversed flow. The inflow boundary condition used in this research is capable of handling reversed flow conditions in ducts. However, the variable exit static pressure boundary condition specified at the exit of the compressor causes the solution to diverge during reversed flow conditions. Due to the presence of swirl, this boundary condition is appropriate for forward flow in the compressor model. Therefore, the variable exit static pressure

boundary condition will need to be modified for reversed flow. A simple test could be added so that when the flow reverses, the exit boundary condition could automatically switch from variable exit static pressure to the inflow/outflow boundary condition specified at the inlet of the computational domain which is capable of reversed flow.

In addition to post-stall analysis, inlet distortion analysis is another avenue of application of this 3-D model. A boundary condition could be used to simulate a steady-state inlet pressure or temperature distortion. A porous wall boundary condition already exists in NPARC. This boundary condition could be used to model distortion screens similar to those used in a test environment.

6.3.4 Implementing Multiple Blade Rows

Another logical step for the expansion and future application of this model is to expand the model to multiple blade rows. This expansion should be validated for pre-stall compressor performance before being extended to post-stall operation. This step may require grid modifications for the rotor/stator, and further refinements may be necessary for expansion into the post-stall operating regimes. Depending on the geometry of the compressor being modeled, volume may have to be added at the exit and/or inlet to produce the desired post-stall operating regime, e.g., surge (refer to Greitzer, Ref. 35, for more information).

6.3.5 Implementing Better Stage Characteristics

Experimental data are usually used to define the compression system characteristics. Analytical techniques, such as the streamline curvature code (Ref. 31), are available for defining the characteristics; however, analytical methods must be correlated to actual test data to ensure the accuracy and consistency of their predictions. Most compression system characteristic information is limited to the pre-stall operating regimes. Little post-stall experimental data exist, especially for high-speed/high-performance compression systems typical of today's gas turbine engines. Therefore, estimates of stage performance in post-stall regions must be made. New tools are being developed to predict both pre-stall and post-stall characteristics in the rotating stall and reverse flow regions (Ref. 36). The specification of the compressor characteristics is imperative for the operation of the 3-D compressor model presented in this report. Theoretical techniques for obtaining compressor characteristics should continue to be matured, improved, and validated. Future experimental endeavors should be aimed toward acquiring accurate post-stall characteristics, as well as pre-stall characteristics.

6.4 IMPLICATIONS FOR 3-D SURGE ANALYSIS

Surge analysis of engine and compression systems is becoming increasingly important to airframe manufacturers as well as engine manufacturers. The implications of surge phenomena on the integration of the engine and airframe are of utmost concern.

The research presented in this report has the potential for being extended to surge cycle analysis. The stage characteristic approach is a proven 1-D methodology for post-stall prediction (Refs. 2 and 5). The extension from 1-D to 3-D will provide a means to investigate the 3-D flow

field in a compressor during surge. Eventually, this type of analysis could be integrated with a structural analysis simulation to investigate the effects of compressor surge on the structural integrity of the airframe.

REFERENCES

1. Garrard, G. D. "ATEC: The Aerodynamic Turbine Engine Code for the Analysis of Transient and Dynamic Gas Turbine Engine System Operations." Ph.D. Dissertation, The University of Tennessee, Knoxville, TN, 1995.

2. Hale, A. A. and Davis, M. W., Jr. "DYNamic Turbine Engine Compressor Code, DYNTECC - Theory and Capabilities." AIAA-92-3190, AIAA/SAE/ASME/ASEE, 28th Joint Propulsion Conference, Nashville, TN, July 1992.

3. Hale, A. A., Davis, M. W., Jr., and Kneile, K. R. "Turbine Engine Analysis Compressor Code: TEACC, Part I: Technical Approach and Steady Results." AIAA- 94-0148, 32nd Aerospace Sciences Meeting and Exhibit, Reno, NV, January 1994.

4. Davis, M. W., Jr. "A Stage-by-Stage Post-Stall Compression System Modeling Technique: Methodology, Validation, and Application." Ph.D. Dissertation, Virginia Polytechnic Institute and State University, Blacksburg, VA, 1986.

5. Davis, M. W., Jr. "Parametric Investigation into the Combined Effects of Pressure and Temperature Distortion on Compression System Stability." AIAA-91-1895, AIAA/SAE/ASME/ASEE, 27th Joint Propulsion Conference, Sacramento, CA, June 1991.

6. Power, G. D. and Cooper, G. K. "NPARC 2.2 - Features and Capabilities." AIAA- 95-2609, 31st AIAA/ASME/SAE/ASEE Joint Propulsion Conference and Exhibit, San Diego, CA, July 1995.

7. Kimzey, W. F. "An Analysis of the Influence of Some External Disturbances on the Aerodynamic Stability of Turbine Engine Axial Flow Fans and Compressors." AEDC-TR-77-80, August 1977.

8. Mazzawy, R. S. "Multiple Segment Parallel Compressor Model for Circumferential Flow Distortion." Transactions of the ASME, *Journal of Engineering for Power*, Vol. 99, April 1977, pp. 288-296.

9. Shahrokhi, K. A. "Application of a Modified Dynamic Compression System Model to a Low-Aspect-Ratio Fan: Effects of Inlet Distortion." Master's Thesis, Vanderbilt University, Nashville, TN, 1995.

10. Lindau, J. W. "Multi-dimensional Dynamic Compression System Modeling." Ph.D. Dissertation, Virginia Polytechnic Institute and State University, Blacksburg, VA, 1995.

11. Escuret, J. F. and Garnier, V. "Numerical Simulations of Surge and Rotating Stall In Multi-Stage Axial-Flow Compressors." AIAA-94-3202, 30th AIAA/ASME/SAE/ASEE Joint Propulsion Conference, Indianapolis, IN, June 1994.

12. Tan, C. S. "Inlet Distortion in Engine on VSTOL Aircraft." Internal MIT Report, Massachusetts Institute of Technology (MIT), 1993.

13. Billet, G., Laval, P., and Chevalier, P. "Numerical Simulation of the Response of an Axial Compressor to a Nonhomogeneous Flow." La Recherche Aerospatiale (English Edition), No. 4, 1985, pp. 19-32.

14. Billet, G., Huard, J., Chevalier, P., and Laval, P. "Experimental and Numerical Study of the Response of an Axial Compressor to Distorted Inlet Flow." Transactions of the ASME, *Journal of Fluids Engineering*, Vol. 110, December 1988, pp. 355-360.

15. Dawes, W. N. "Toward Improved Throughflow Capability: The Use of Three- Dimensional Viscous Flow Solvers in a Multistage Environment." Transactions of the ASME, *Journal of Turbomachinery*, Vol. 114, January 1992, pp. 8-17.

16. Denton, J. D. "The Calculation of Three-Dimensional Viscous Flow Through Multistage Turbomachines." Transactions of the ASME, *Journal of Turbomachinery*, Vol. 114, January 1992, pp. 18-26.

17. Adamczyk, J. J. "Model Equation for Simulating Flows in Multistage Turbomachinery." NASA Technical Memorandum 86869, 1984.

18. Mulac, R. A. and Adamczyk, J. J. "The Numerical Simulation of a High-Speed Axial Flow Compressor." Transactions of the ASME, *Journal of Turbomachinery*, Vol. 114, July 1992, pp. 517-527.

19. Subramanian, S. V. and Bozzola, R. "Numerical Simulation of Three-Dimensional Flow Fields in Turbomachinery Blade Rows Using the Compressible Navier-Stokes Equations." AIAA-87-1314, AIAA 19th Fluid Dynamics, Plasma Dynamics and Lasers Conference, Honolulu, HA, June 1987.

20. Greitzer, E. M. and Strand, T. "Asymmetric Swirling Flows in Turbomachine Annuli." Transactions of the ASME, *Journal of Engineering for Power*, Vol. 100, October 1978, pp. 618-629.

21. Power, G. D. and Cooper, G. K. "NPARC 2.2 - Features and Capabilities." AIAA- 95-2609, 31st AIAA/ASME/SAE/ASEE Joint Propulsion Conference and Exhibit, San Diego, CA, July 1995.

22. Pulliam, T. H. and Steger, J. L. "Implicit Finite-Difference Simulations of Three Dimensional Compressible Flow." *AIAA Journal*, Vol. 18, No. 2, February 1980, pp. 159-167.

23. Pulliam, T. H. "Euler and Thin Layer Navier-Stokes Codes: ARC2D, ARC3D." Notes for Computational Fluid Dynamics User's Workshop, The University of Tennessee Space Institute, Tullahoma, TN, UTSI Publication E02-4005-023- 84, March 12-16, 1984, pp. 15.1-15.85.

24. Beam, R. and Warming, R. F. "An Implicit Finite Difference Algorithm for Hyperbolic Systems in Conservation Law Form." *Journal of Computational Physics*, Vol. 22, No. 1, September 1976, pp. 87-110.

25. Power, G. D. and Prufert, M. B. "Computational Evaluation of Diffuser Performance in a Turbine Engine Altitude Test Cell." AIAA-96-0498, 34th AIAA Aerospace Sciences Meeting and Exhibit, Reno, NV, January 1996.

26. Dudek, J. C., Georgiadis, N. J., and Yoder, D. A. "Calculation of Turbulent Subsonic Diffuser Flows Using the NPARC Navier-Stokes Code." AIAA-96-0497, 34th AIAA Aerospace Sciences Meeting and Exhibit, Reno, NV, January 1996.

27. Nobel, T. P., Wooden, P. A., and Arledge, R. G. "Experimental Thrust Reverser Design with Computational Analysis." AIAA-94-0021, 32nd AIAA Aerospace Sciences Meeting and Exhibit, Reno, NV, January 1994.

28. Bartlett, C. S. and Phares, W. J. "Icing Testing of a Large Full-Scale Inlet at the Arnold Engineering Development Center." AIAA-93-0299, 31st AIAA Aerospace Sciences Meeting and Exhibit, Reno, NV, January 1993.

29. Power, G. D. and Heikkinen, B. D. "CFD Applications in an Aeropropulsion Test Environment." AIAA-93-1924, 29th AIAA/SAE/ASME/ASEE Joint Propulsion Conference and Exhibit, Monterey, CA, June 1993.

30. Akima, H. "A New Method of Interpolation and Smooth Curve Fitting Based on Local Procedures." *Journal of the Association for Computing Machinery*, Vol. 17, No. 4, October 1970, pp. 589-602.

31. DYNATECH R/D Company. "HT0300 - A Computer Program for the Design and Analysis of Axial Turbomachinery." Cambridge, MA, March 1970.

32. Seyler, D. R. and Gostelow, J. P. "Single Stage Experimental Evaluation of High Mach Number Compressor Rotor Blading: Part 2 - Performance of Rotor 1B." NASA CR-54582, September 1967.

33. Thompson, J. W. and Abernethy, R. B. "Handbook of Uncertainty in Gas Turbine Measurements." AEDC-TR-73-5, February 1973.

34. Hale, A. A. "A Three-Dimensional Turbine Engine Analysis Compressor Code (TEACC) for Steady-State Inlet Distortion." Ph.D. Dissertation, Virginia Polytechnic Institute and State University, Blacksburg, VA, 1996.

35. Greitzer, E. M. "Surge and Rotating Stall in Axial Flow Compressors - Part I: Theoretical Compression System Model." Transactions of the ASME, *Journal of Engineering for Power*, Vol. 98, No. 2, April 1976, pp. 190-198.

36. Bloch, G. S. and O'Brien, W. F. "A Wide-Range Axial-Flow Compressor Stage Performance Model." ASME-92-GT-58, International Gas Turbine and Aeroengine Congress and Exposition, Cologne, Germany, June 1992.

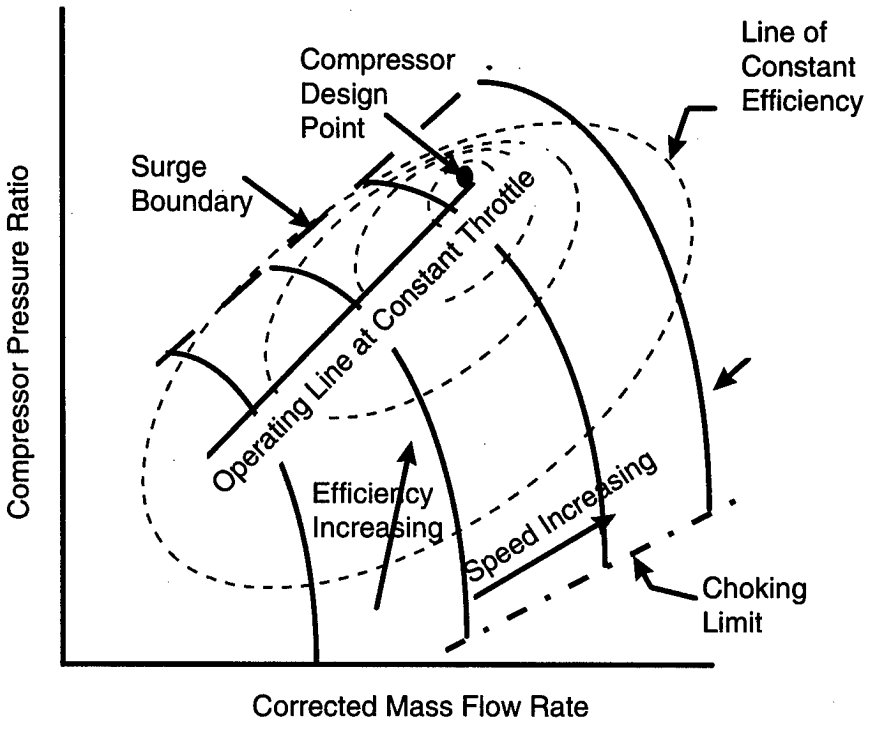

Figure 1. A representative compressor performance map showing lines of constant corrected speed, efficiency, and throttle.

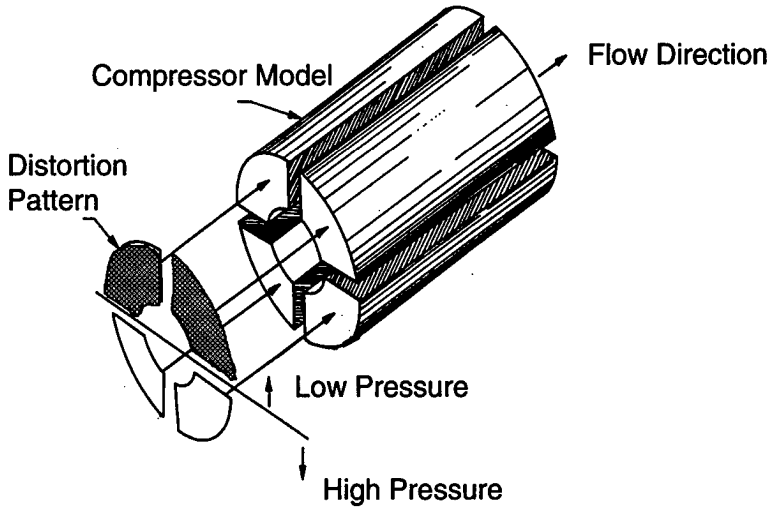

Figure 2. Example of the parallel compressor theory concept with circumferential segments and an applied inlet distortion.

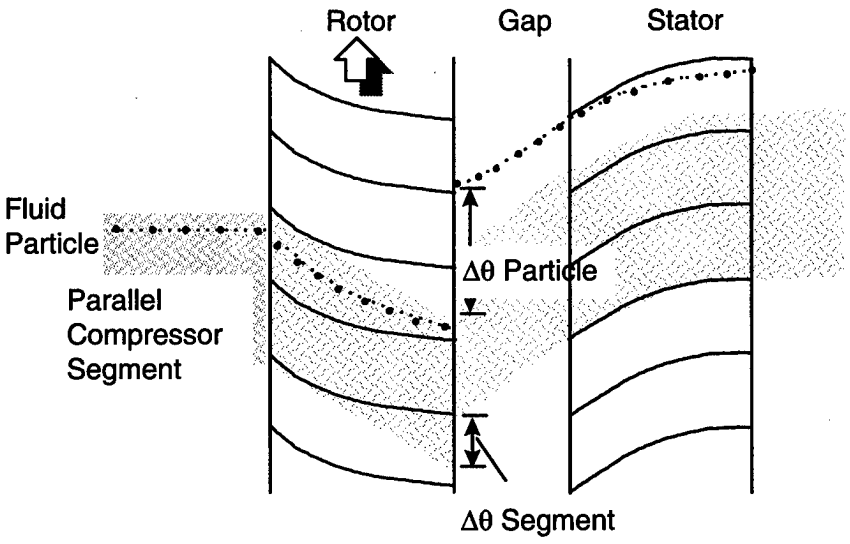

Figure 3. Segment and particle circumferential displacement through compressor in Mazzawy's model.

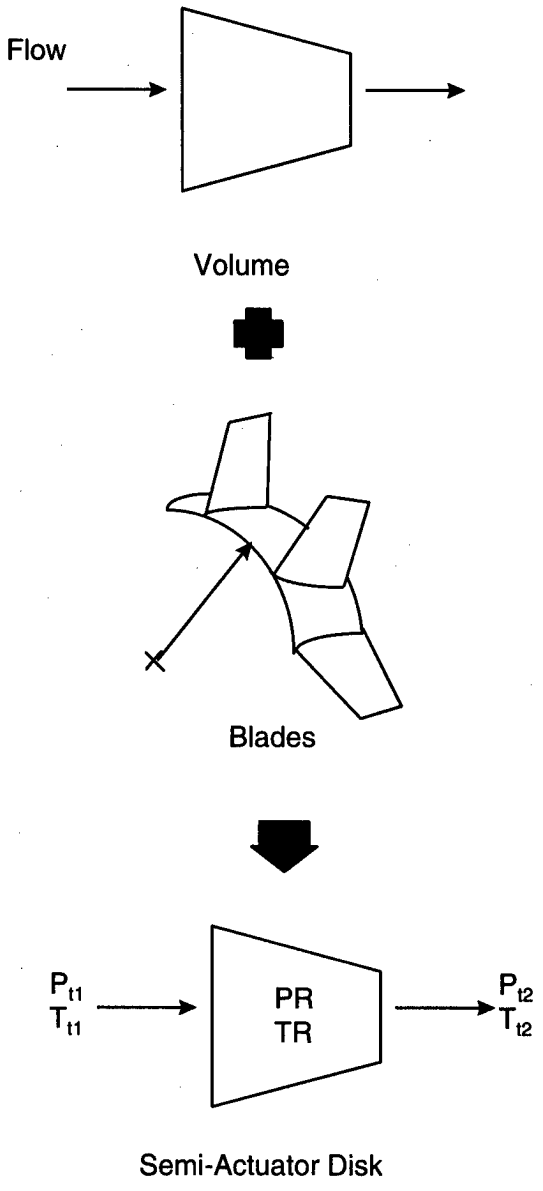

Figure 4. Semi-actuator disk methodology.

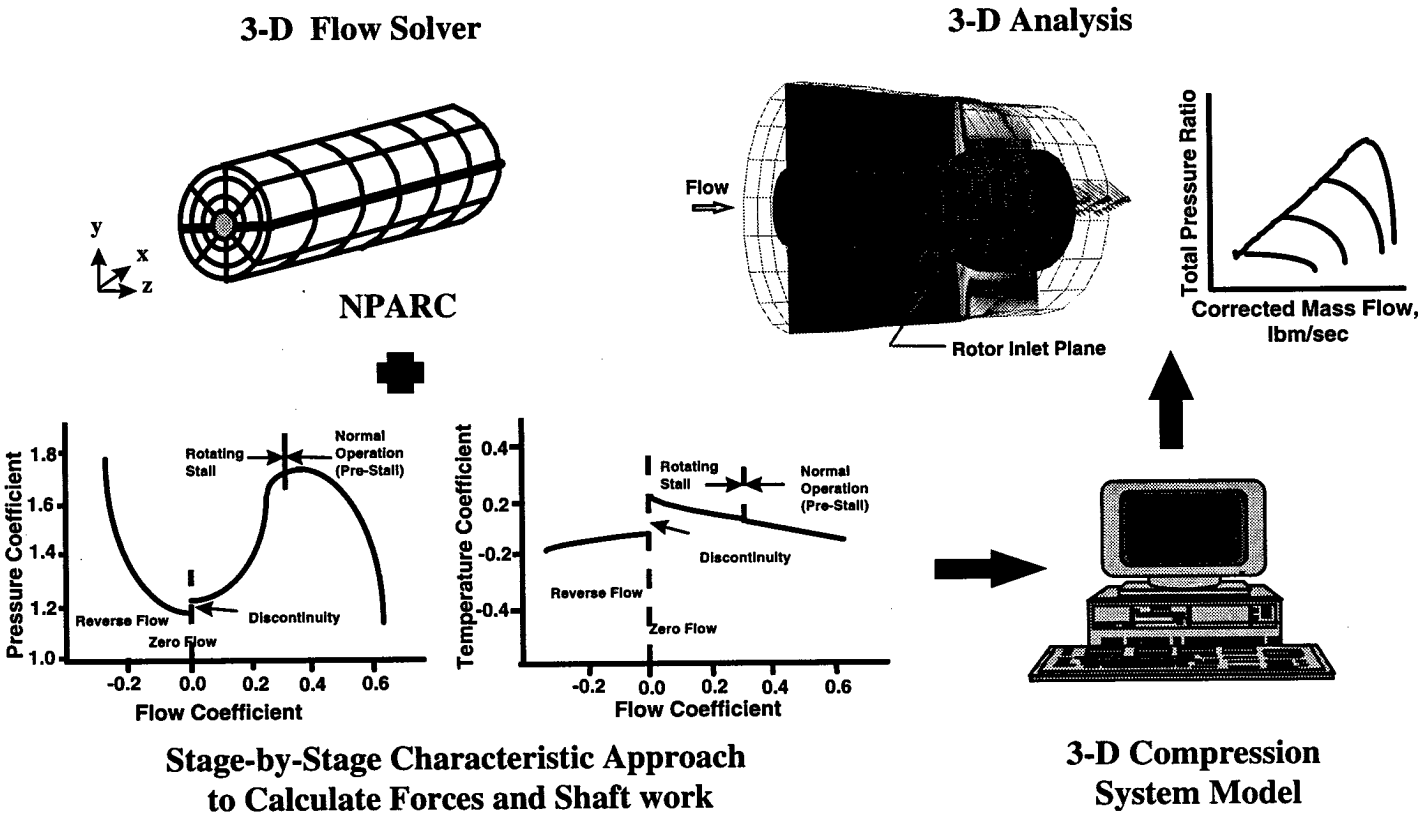

Figure 5. Conceptual approach for constructing the 3-D compression system model.

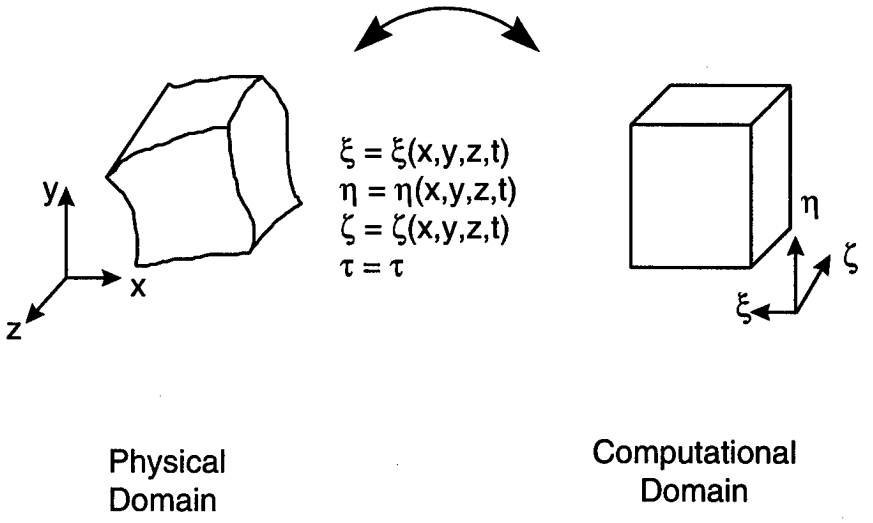

Figure 6. Transformation from physical space to computational space.

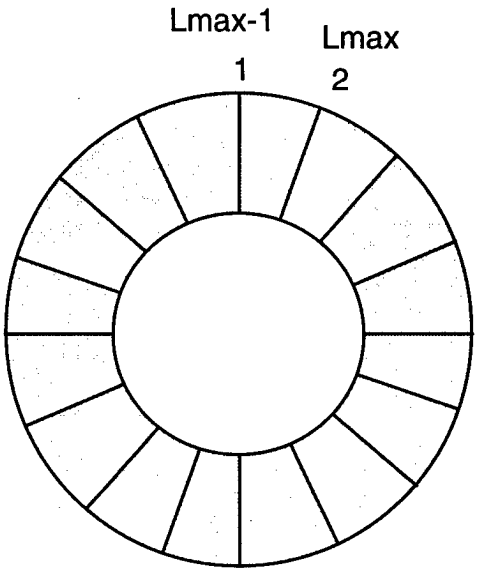

a. Wrap-around boundary

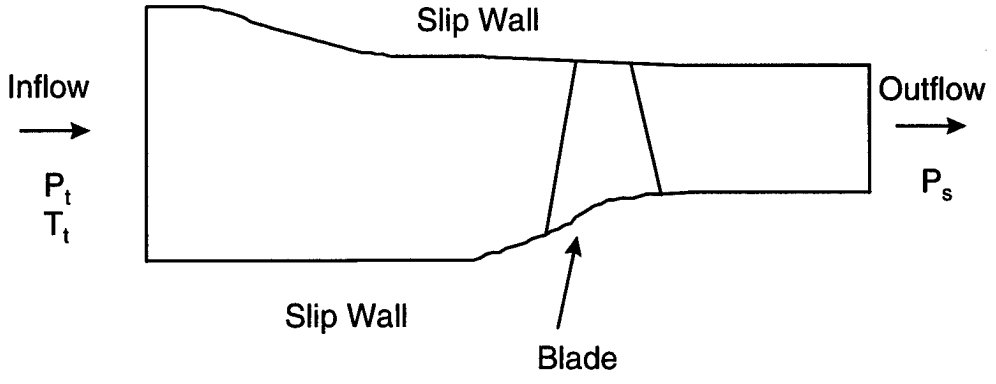

b. Inlet, exit, and wall boundaries

Figure 7. Physical and computational boundaries.

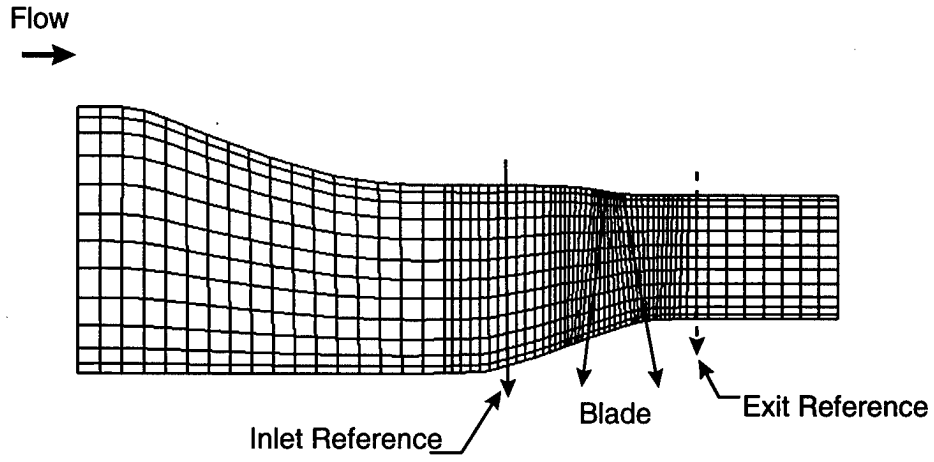

Figure 8. Axial-radial view of Rotor 1B grid, 69×13×26.

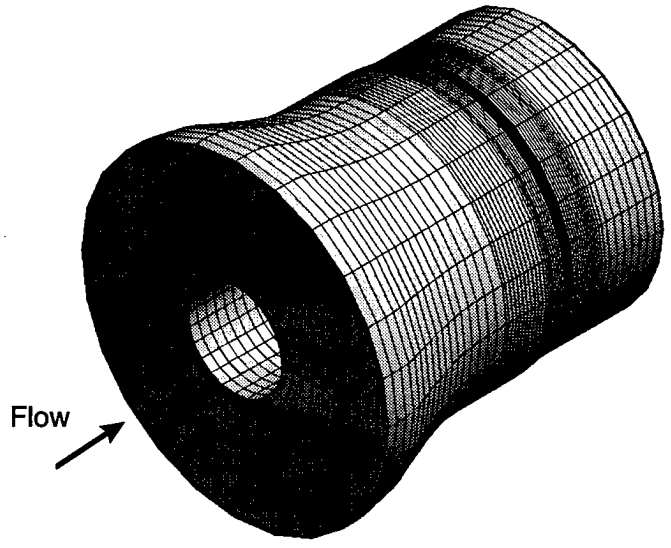

Figure 9. Three-dimensional computational grid, 69×13×26, for Rotor 1B.

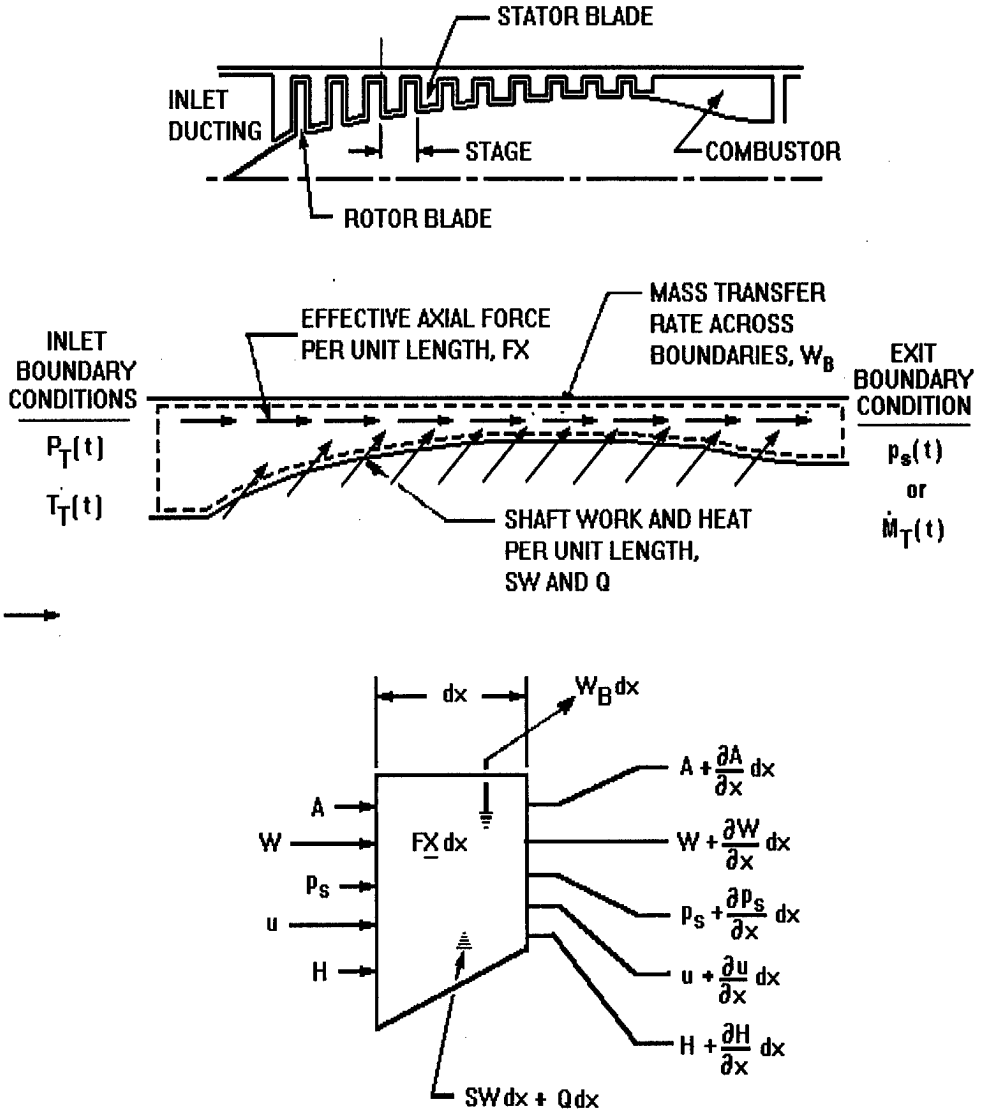

Figure 10. DYNTECC control volume approach.

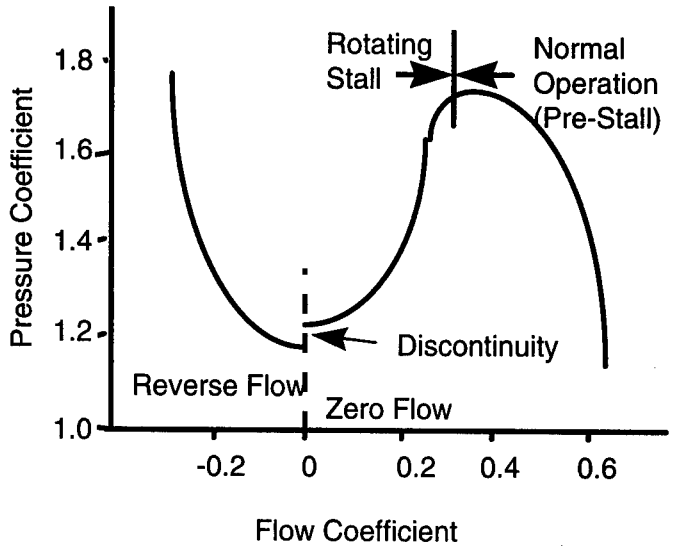

a. Pressure coefficient, Ψ^P, versus flow coefficient, Φ

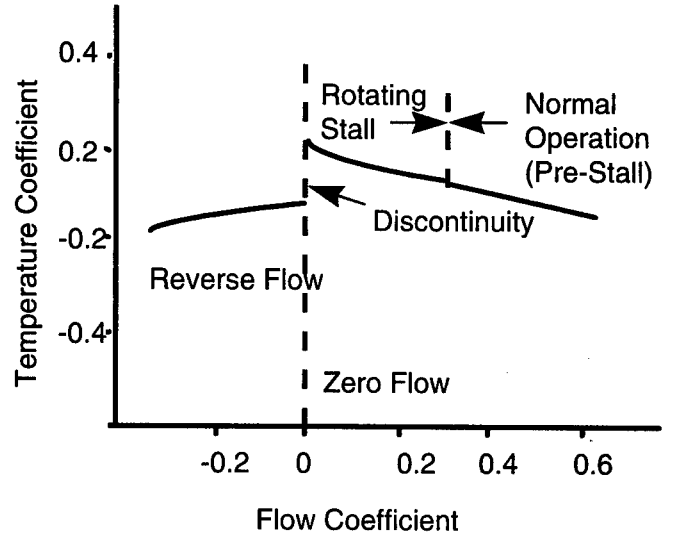

b. Temperature coefficient, Ψ^T, versus flow coefficient, Φ

Figure 11. Typical compressor characteristics.

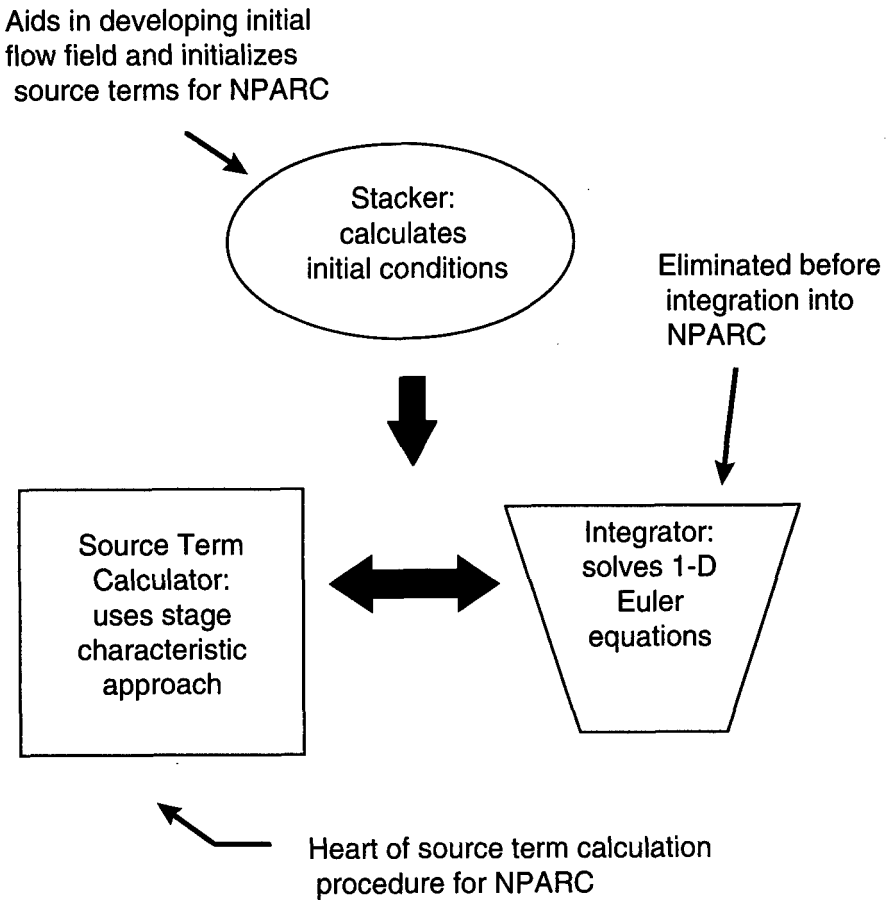

Figure 12. Primary components and overall code structure of DYNTECC.

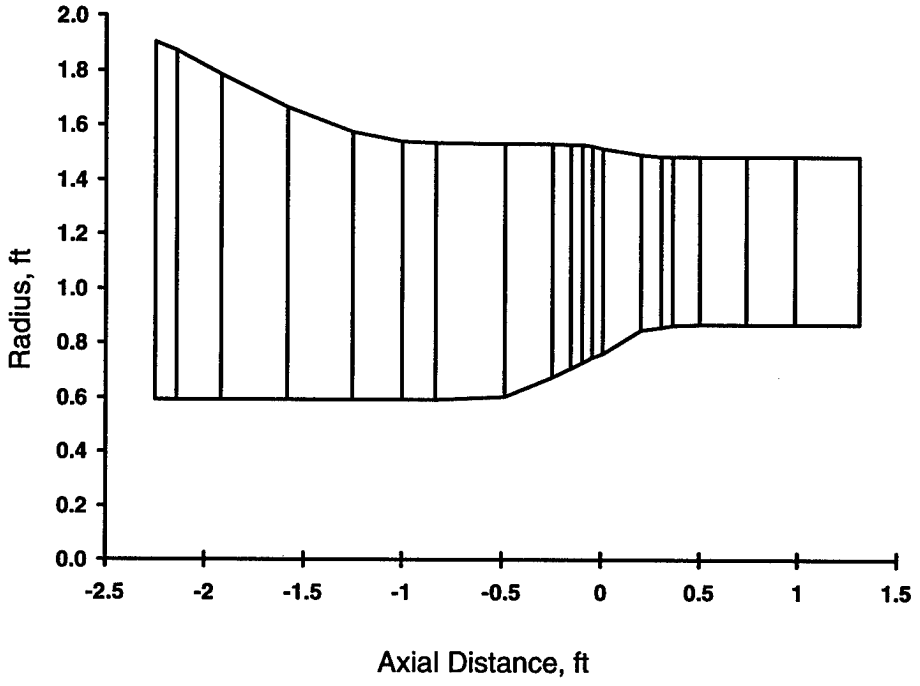

Figure 13. Simple grid for Rotor 1B used by stage characteristic approach and DYNTECC.

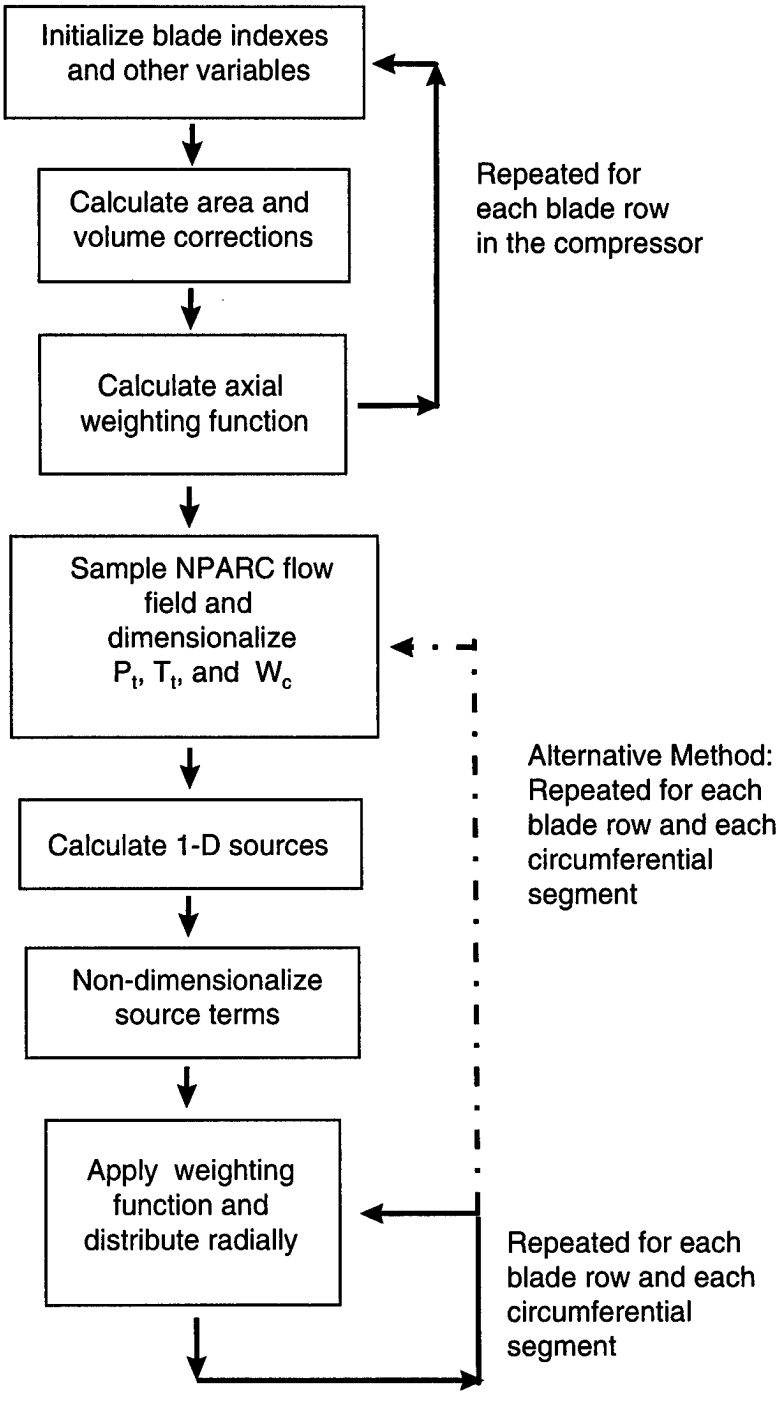

Figure 14. Block diagram of 3-D source calculations.

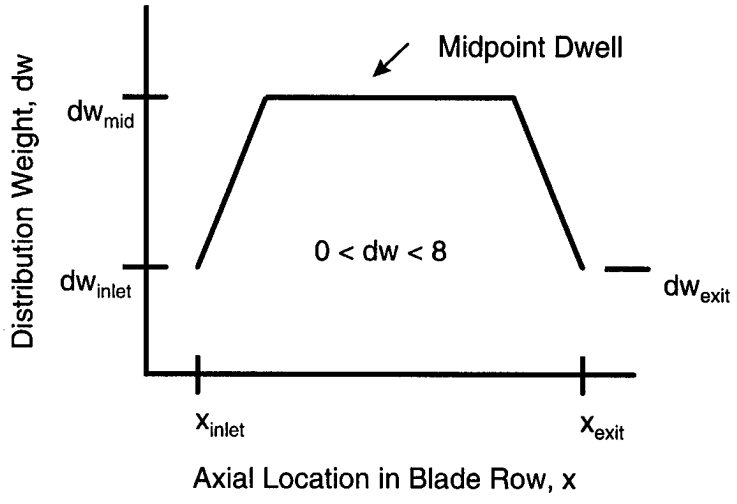

a. Typical axial distribution shape

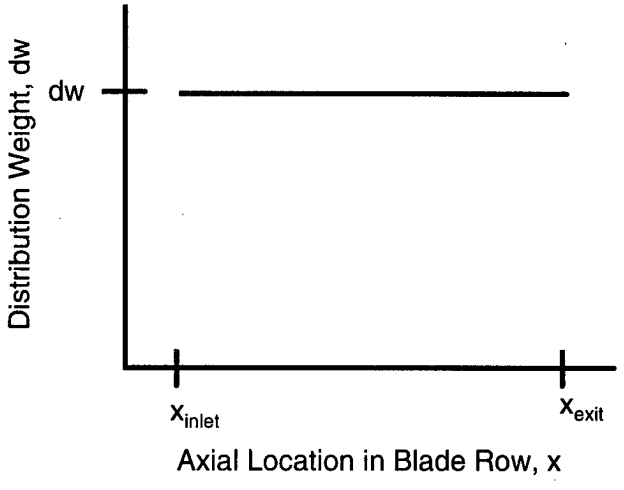

b. Axial distribution shape for best convergence rates

Figure 15. Source weighting technique applied axially to each blade row.

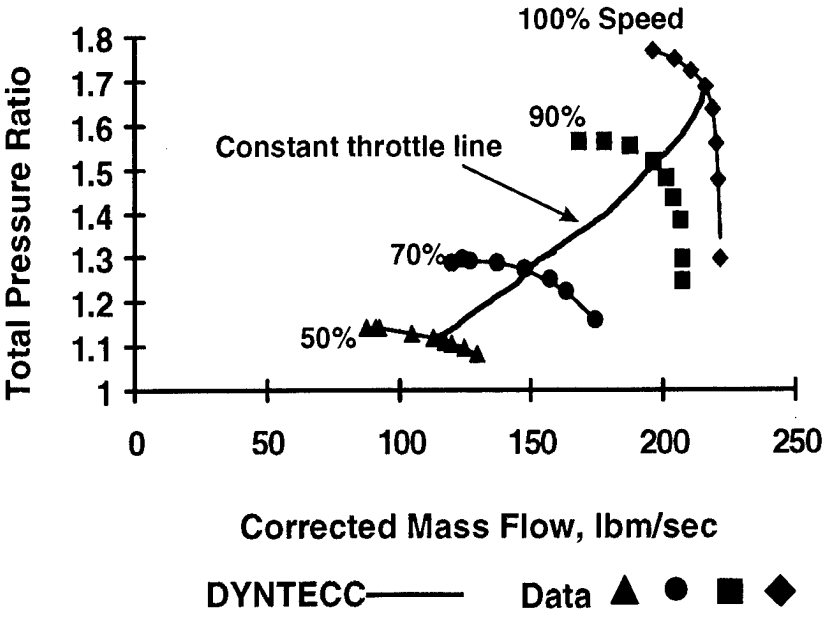

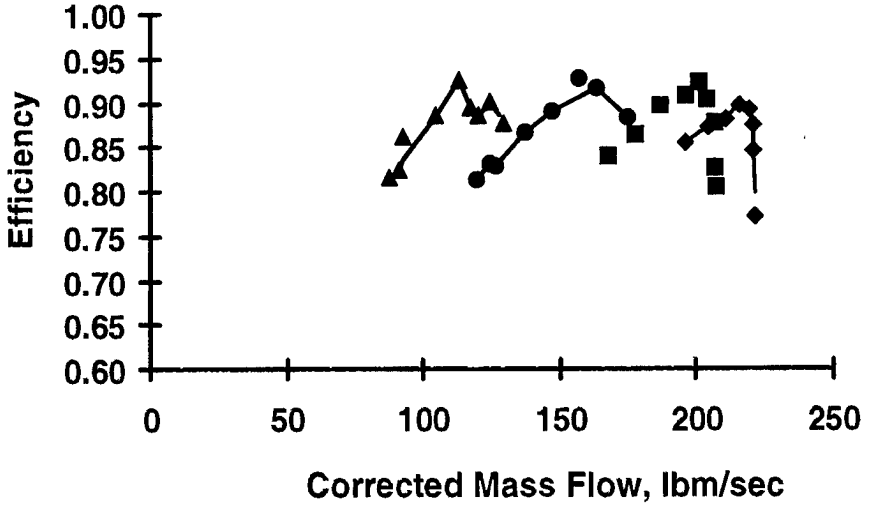

Figure 16. Verfication of stage characteristic approach using DYNTECC.

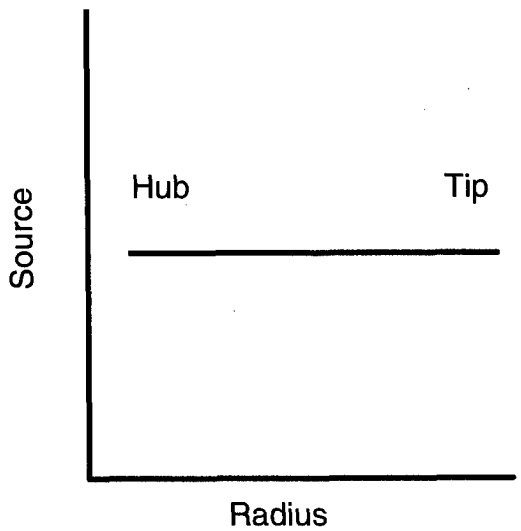

Figure 17. Uniform (slug) source profile.

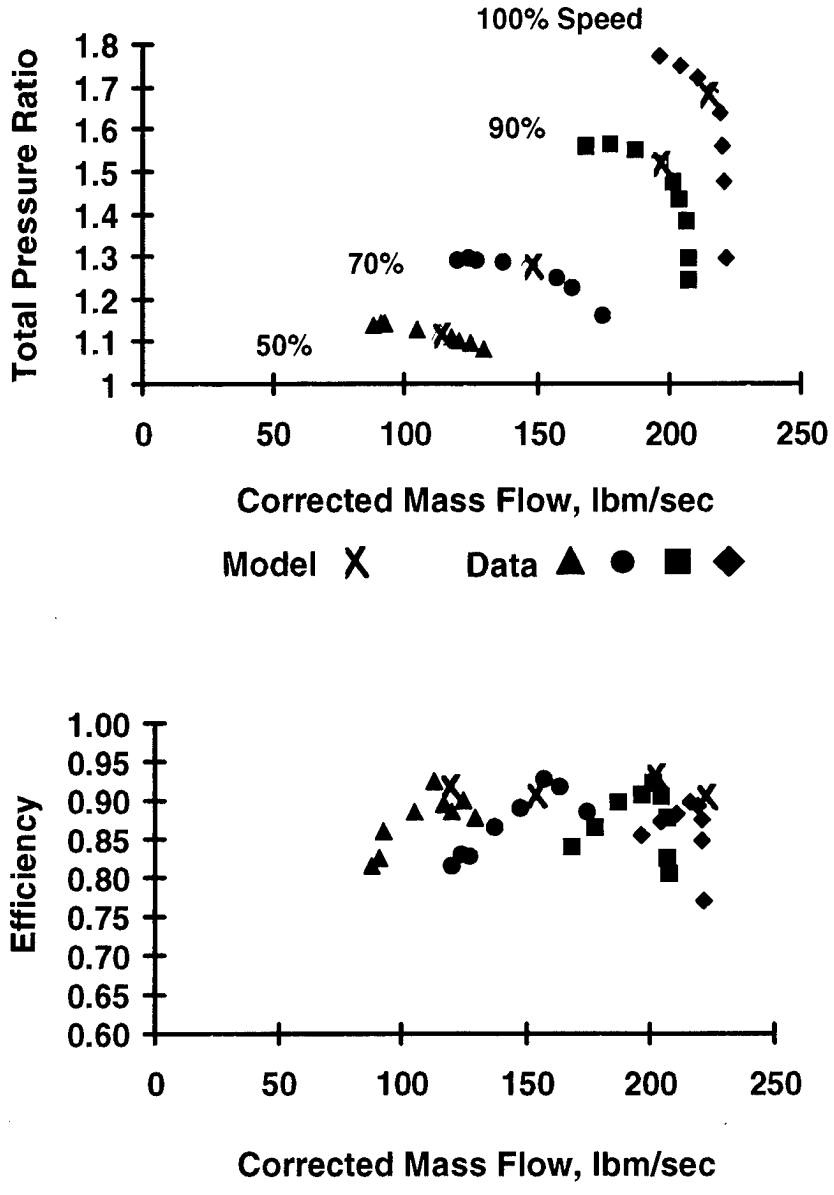

Figure 18. Overall constant throttle line performance using a uniform radial distribution of sources.

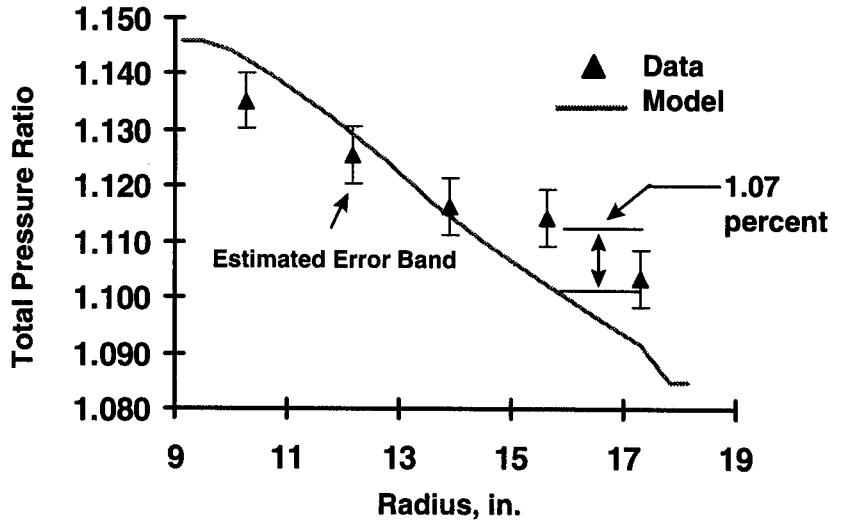

a. Total pressure ratio as a function of radius

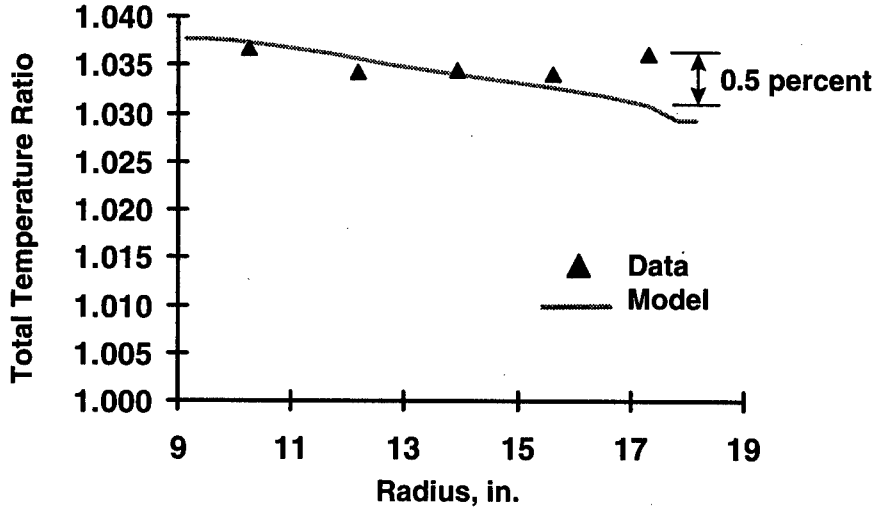

b. Temperature ratio as a function of radius

Figure 19. Radial comparisons of results and experimental data on the constant throttle line at 50-percent speed using a uniform radial distribution of sources.

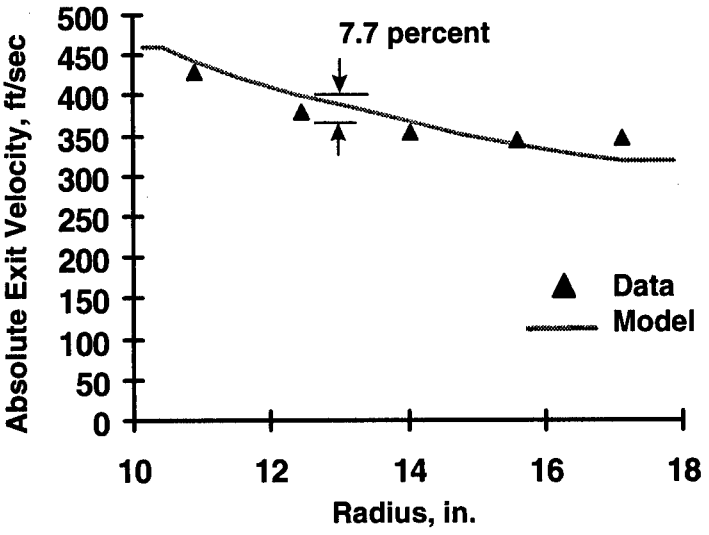

a. Absolute exit velocity as a function of radius

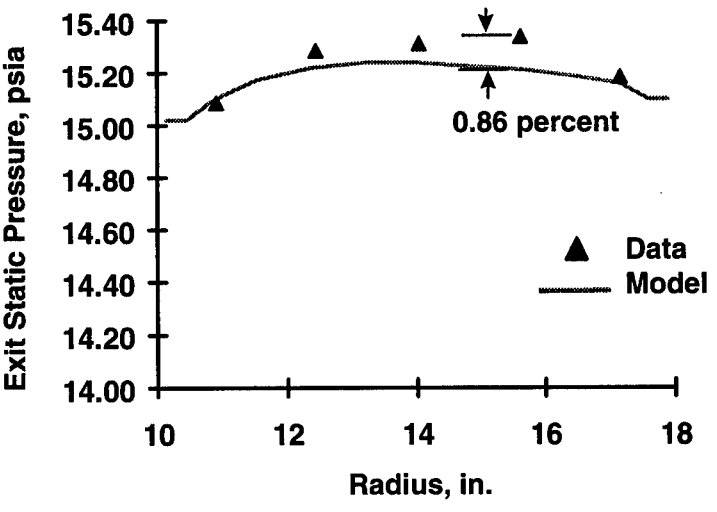

b. Exit static pressure as a function of radius

Figure 20. Additional typical radial comparisons of results and experimental data on the constant throttle line at 50-percent speed using a uniform radial distribution of sources.

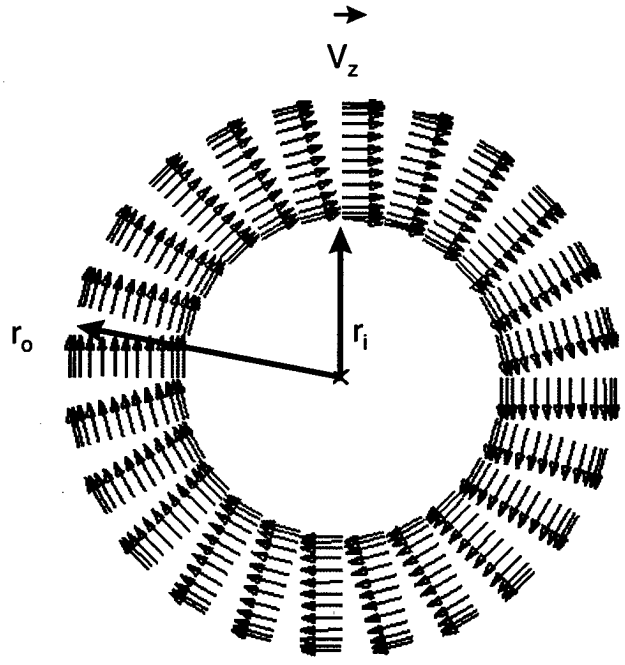

Note: Flow direction through the compressor is into the page.

Figure 21. Typical swirl velocities at the compressor exit as predicted by the 3-D model.

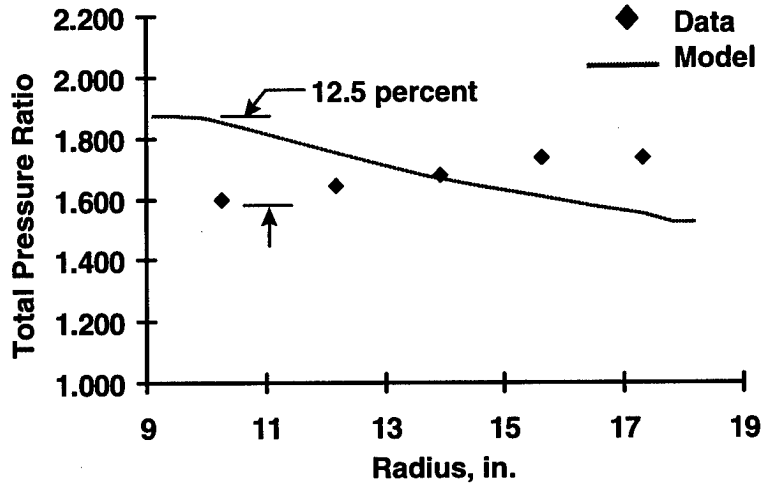

a. Total pressure ratio as a function of radius

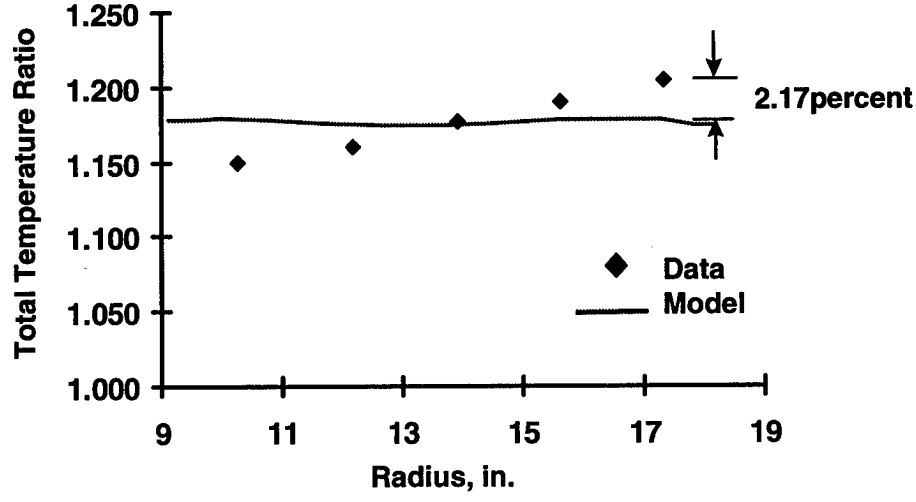

b. Total temperature ratio as a function of radius

Figure 22. Radial comparisons of results and experimental data on the constant throttle line at 100-percent speed using a uniform radial distribution of sources.

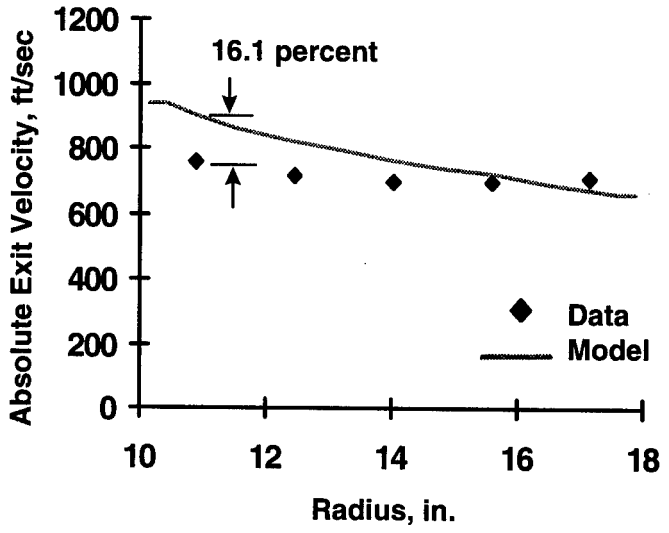

a. Absolute exit velocity as a function of radius

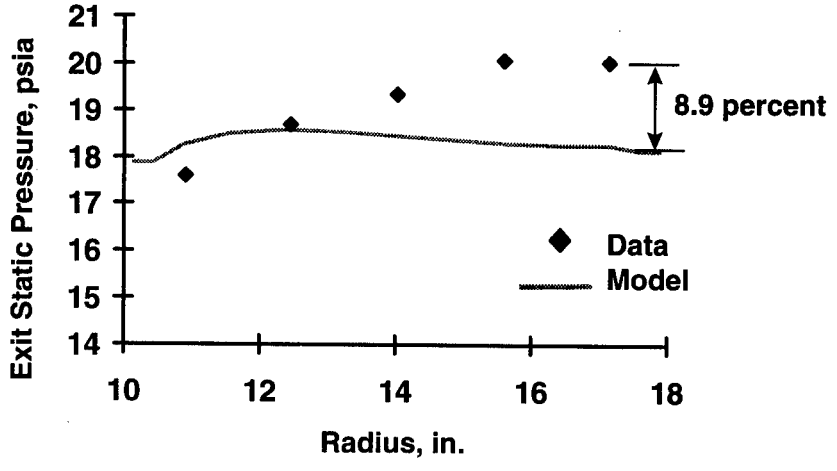

b. Exit static pressure as a function of radius

Figure 23. Additional typical radial comparisons of results and experimental data on the constant throttle line at 100-percent speed using a uniform radial distribution of sources.

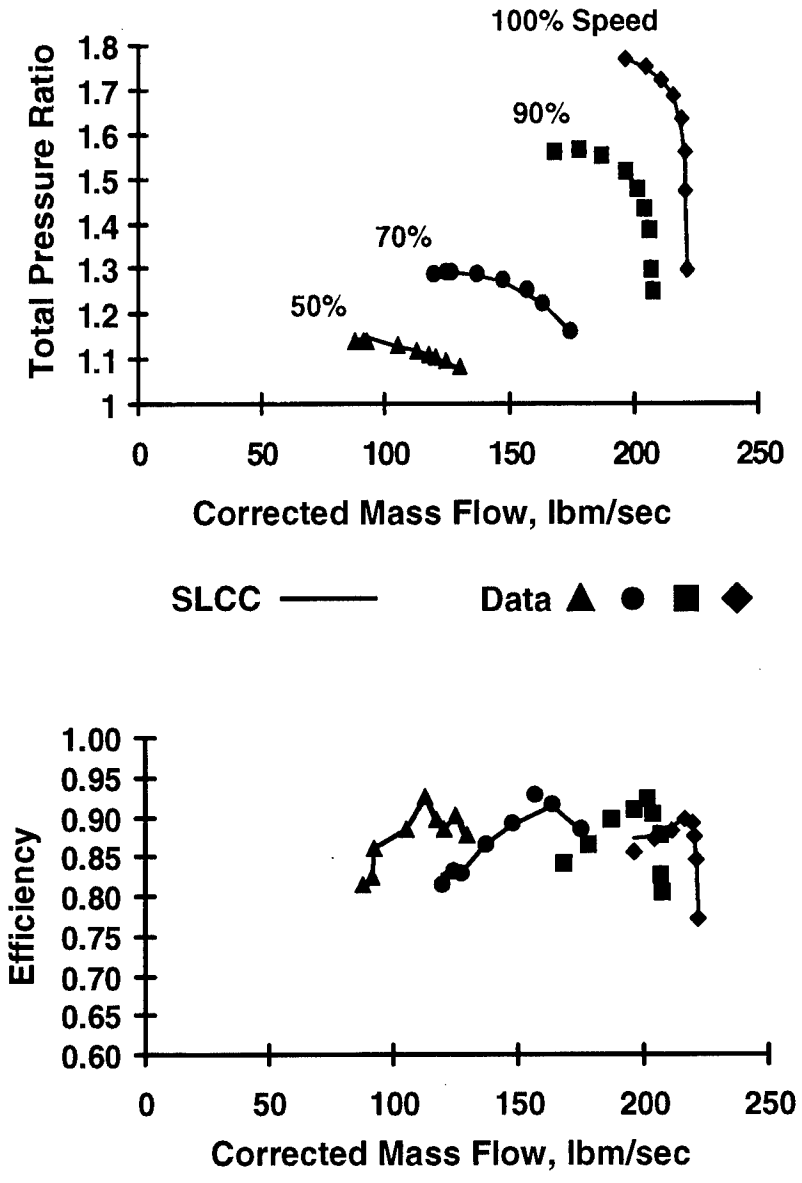

Figure 24. Overall verification of the streamline curvature code (SLCC) as an adequate means of investigating radial distributions of source terms.

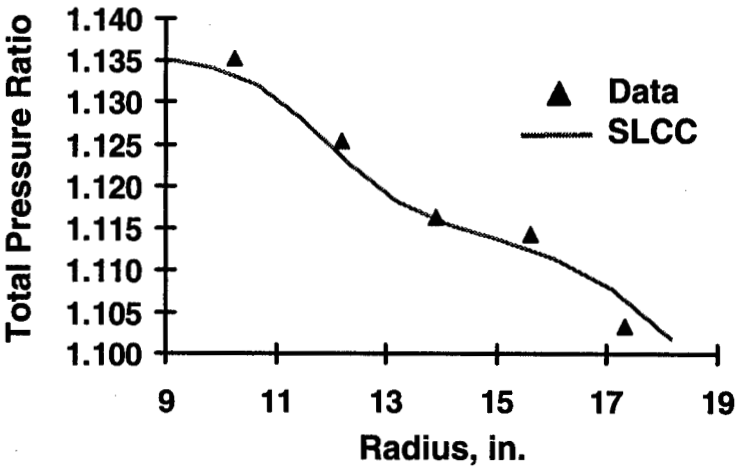

a. Total pressure ratio as a function of radius

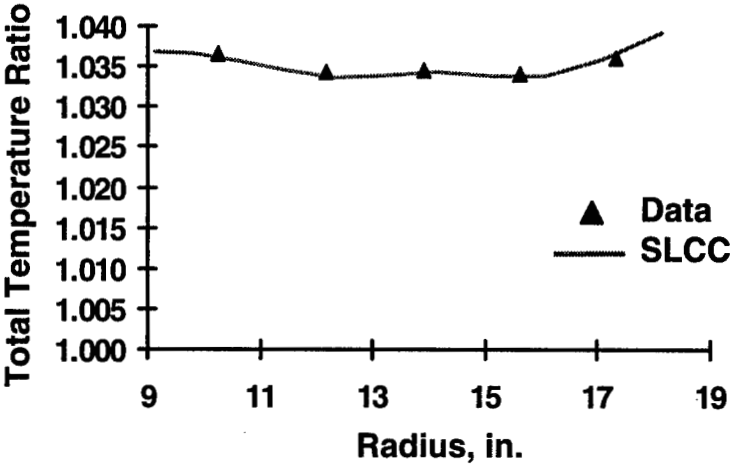

b. Total temperature ratio as a function of radius

Figure 25. Radial verification of the streamline curvature code (SLCC) on the constant throttle line at 50-percent speed.

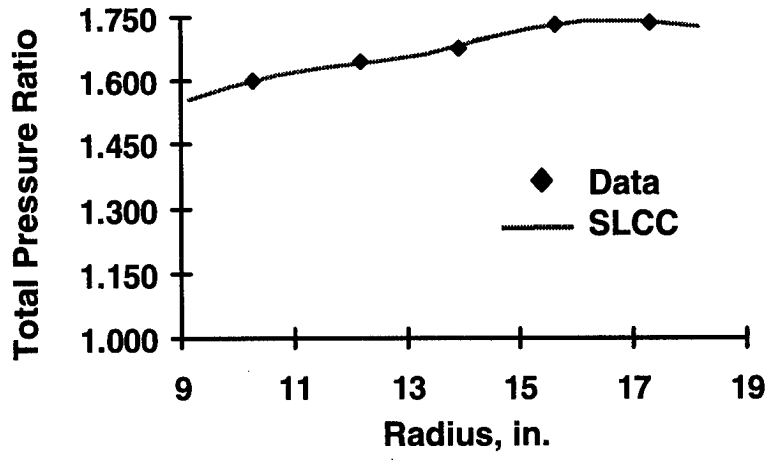

a. Total pressure ratio as a function of radius

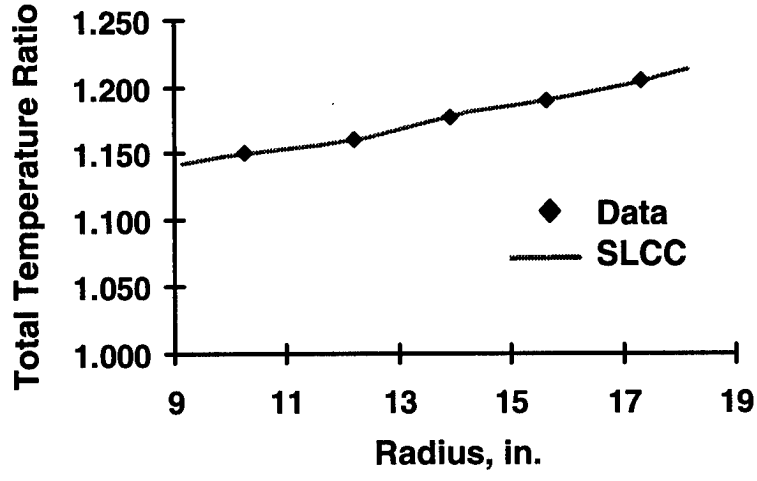

b. Total temperature ratio as a function of radius

Figure 26. Radial verification of the streamline curvature code (SLCC) on the constant throttle line at 100-percent speed.

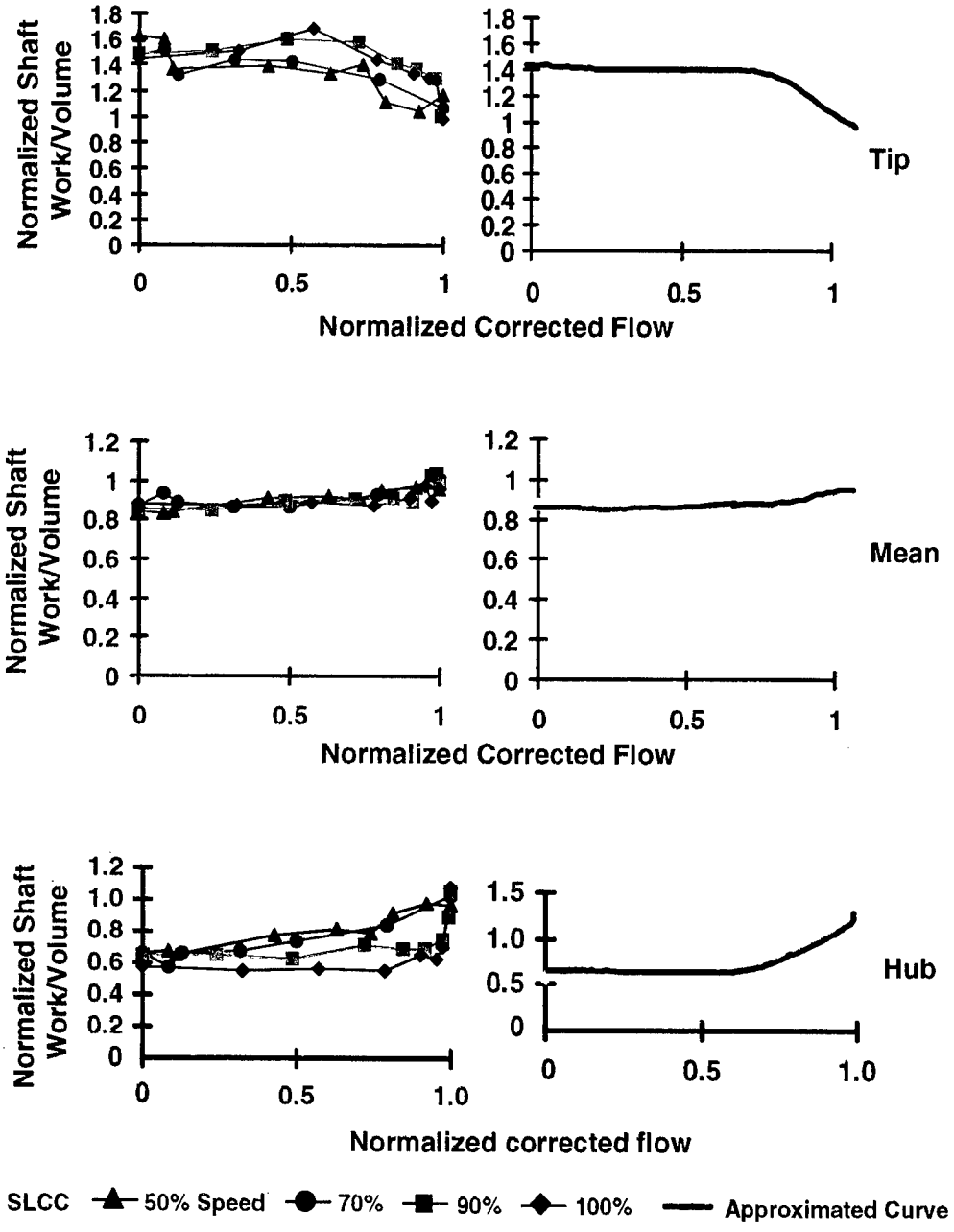

a. Normalized shaft work and approximated curves on per volume basis

Figure 27. Source term correlation based on collapse in speed found from streamline curvature code solutions.

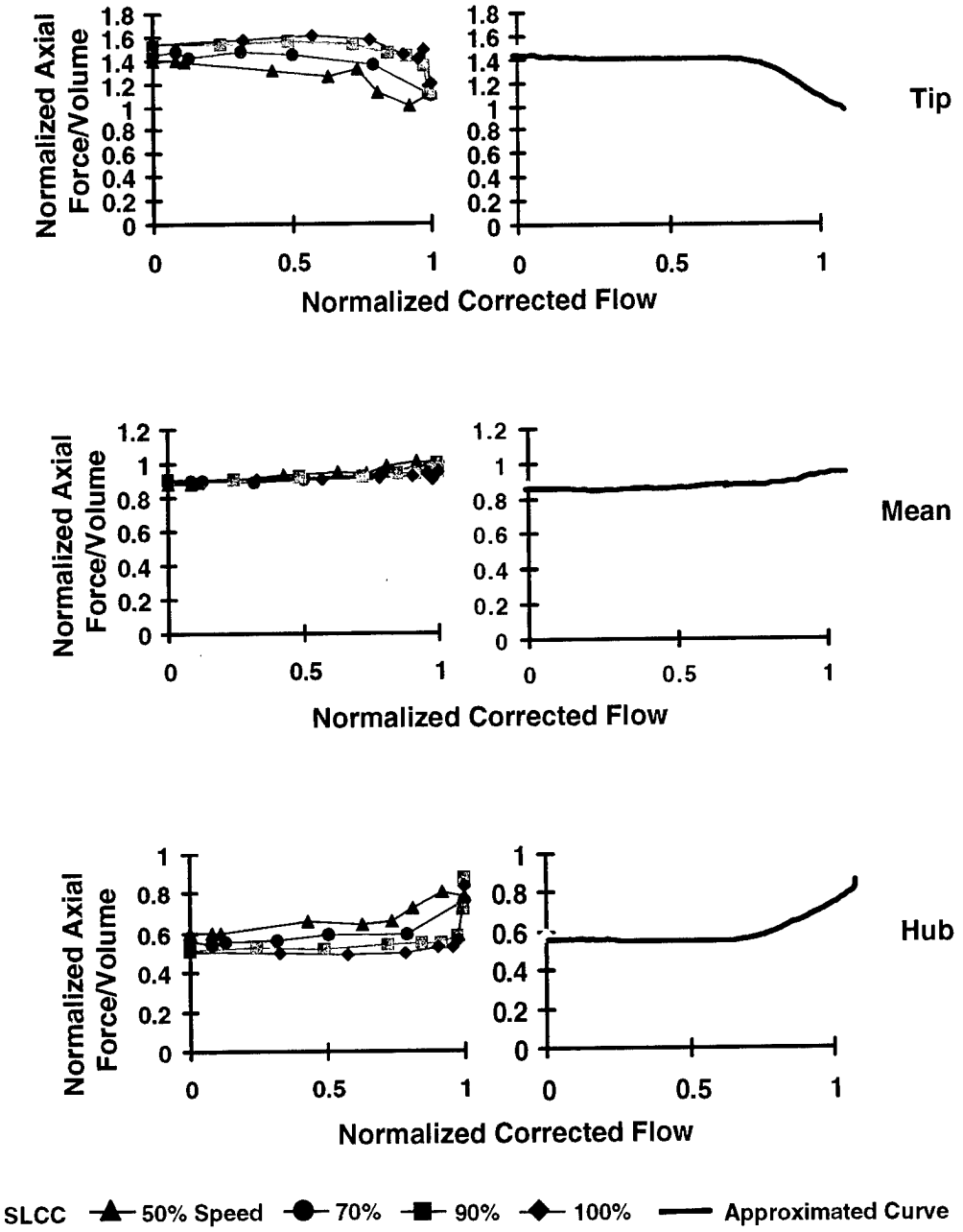

b. Normalized axial force on per volume basis
Figure 27. Continued.

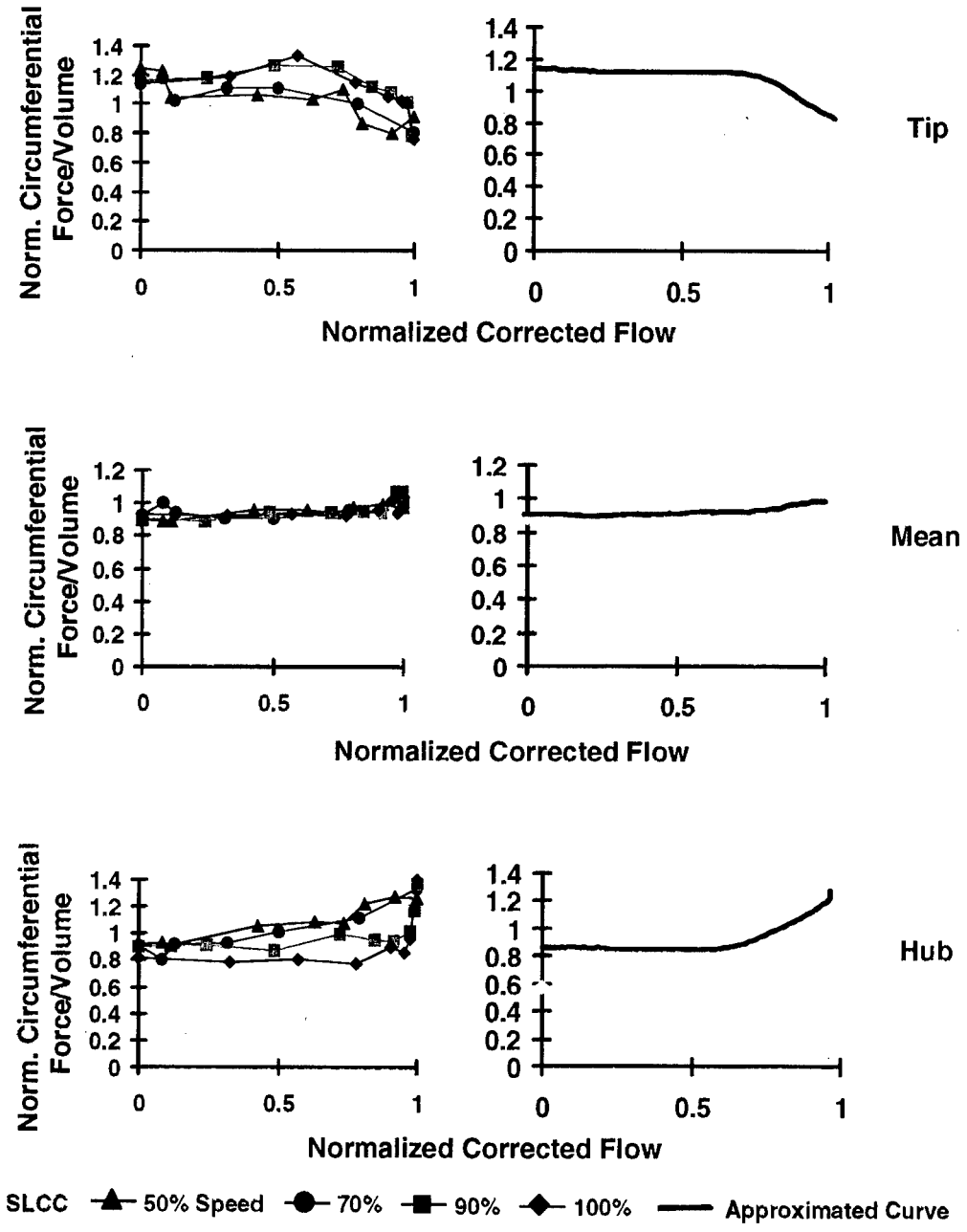

c. Normalized circumferential force on per volume basis
Figure 27. Concluded.

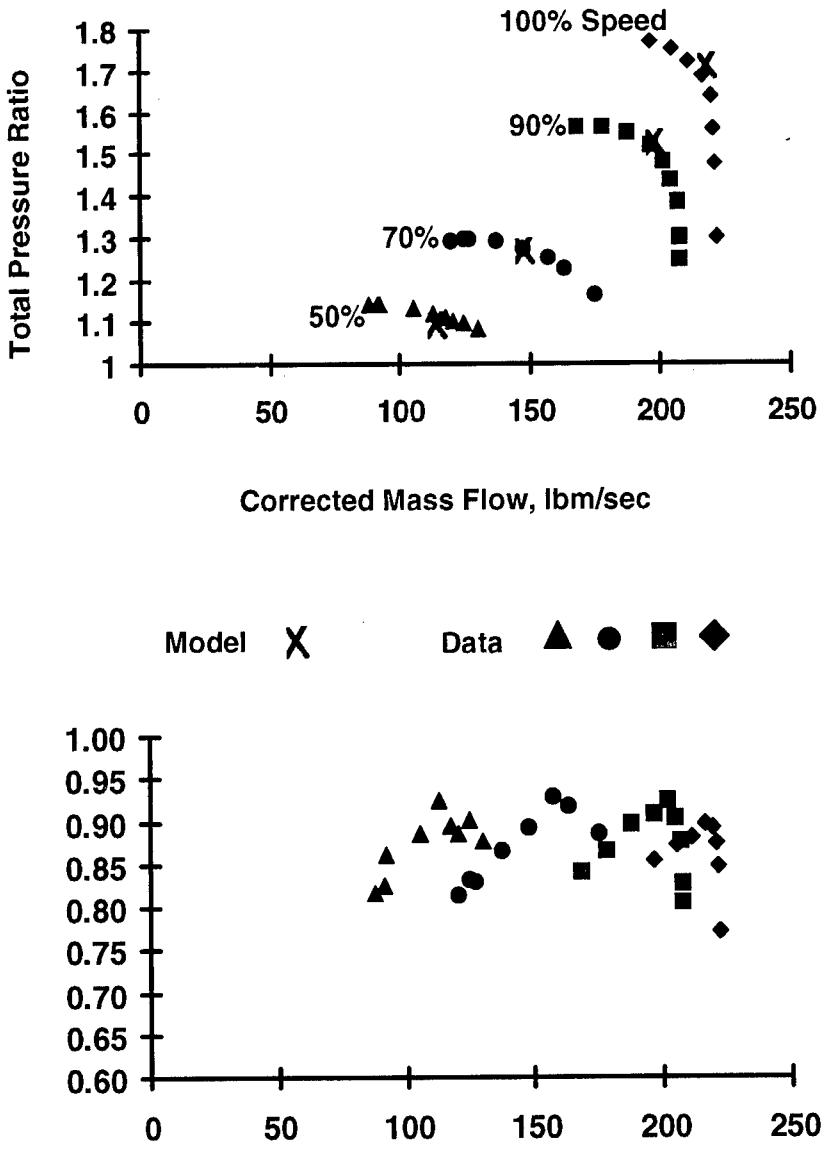

Figure 28. Overall constant throttle line performance using an interpolated radial distribution of sources based on a collapse in speed.

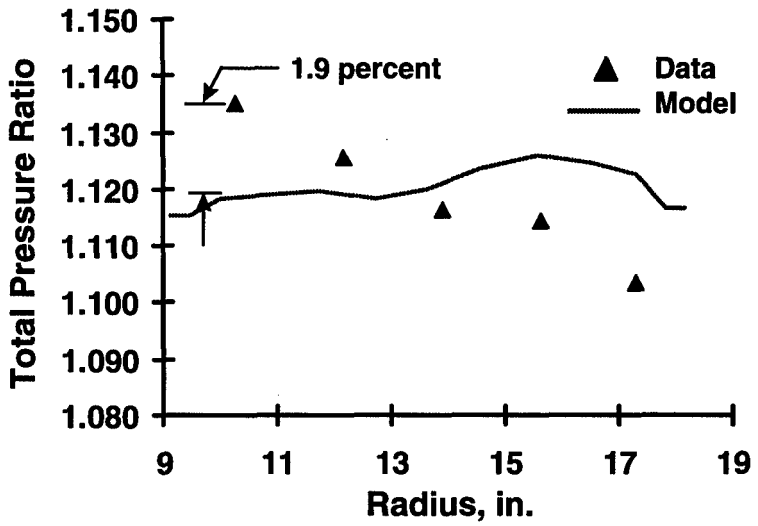

a. Total pressure ratio as a function of radius

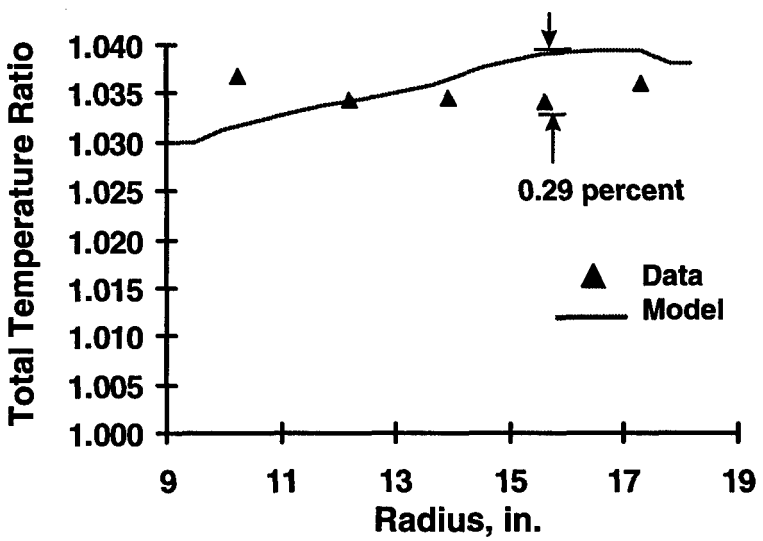

b. Total temperature ratio as a function of radius

Figure 29. Radial comparisons of results and experimental data on the constant throttle line at 50-percent speed using an interpolated radial distribution of sources based on a collapse in speed.

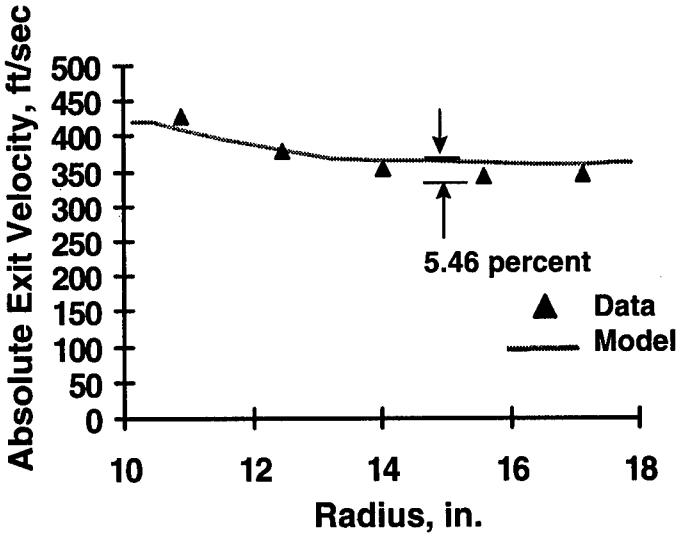

a. Absolute exit velocity as a function of radius

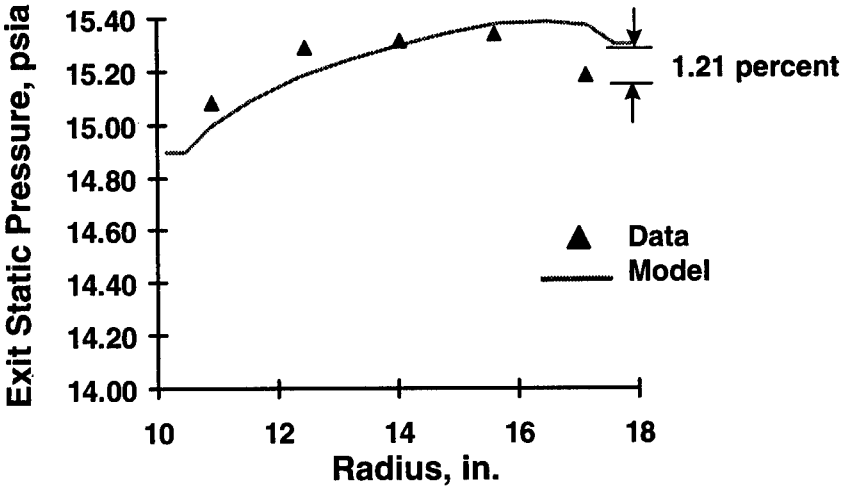

b. Exit static pressure as a function of radius

Figure 30. Additional typical radial comparisons of results and experimental data on the constant throttle line at 50-percent speed using an interpolated radial distribution of sources.

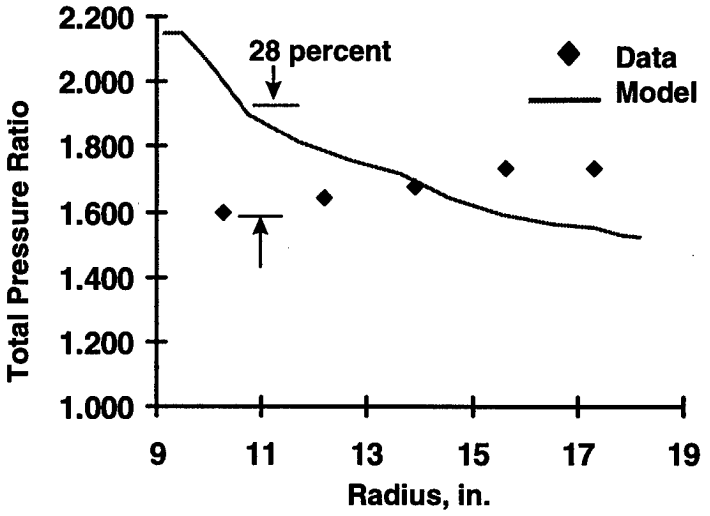

a. Total pressure ratio as a function of radius

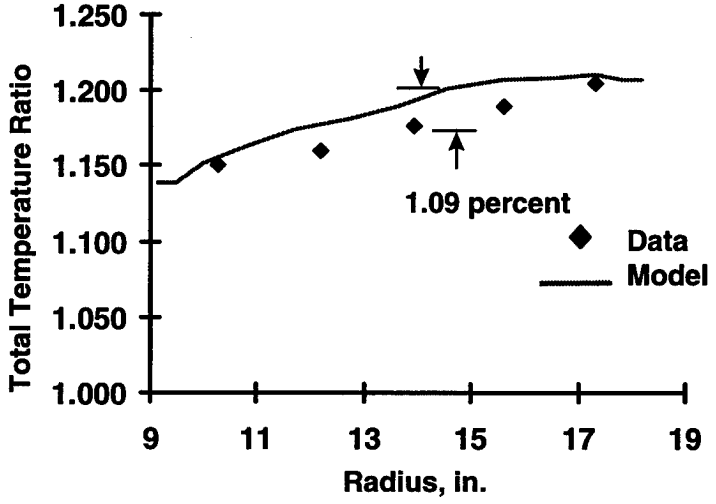

b. Total temperature ratio as a function of radius

Figure 31. Radial comparisons of results and experimental data on the constant throttle line at 100-percent speed using an interpolated radial distribution of sources based on a collapse in speed.

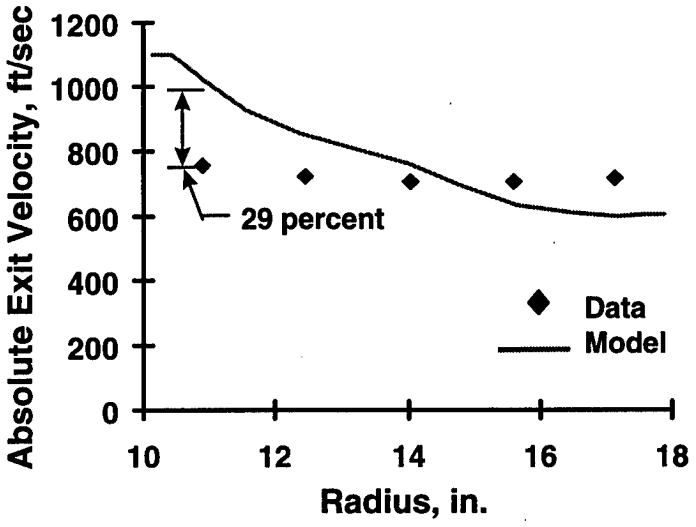

a. Absolute exit velocity as a function of radius

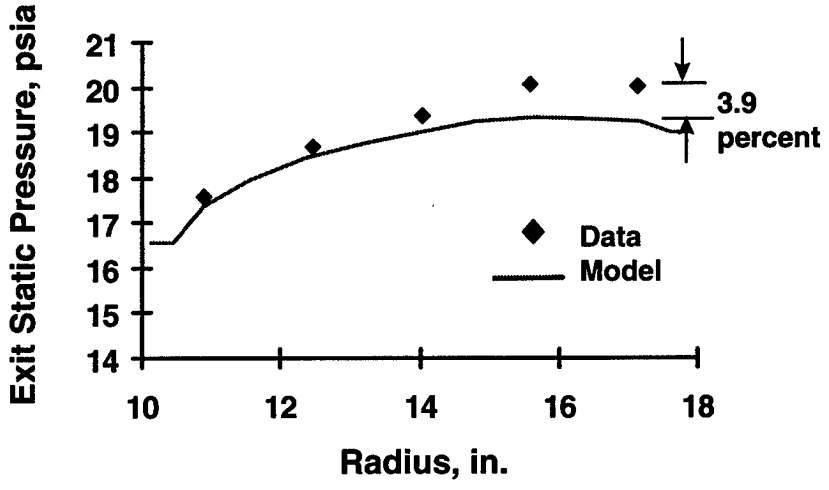

b. Exit static pressure as a function of radius

Figure 32. Additional typical radial comparisons of results and experimental data on the constant throttle line at 100-percent speed using an interpolated radial distribution of sources.

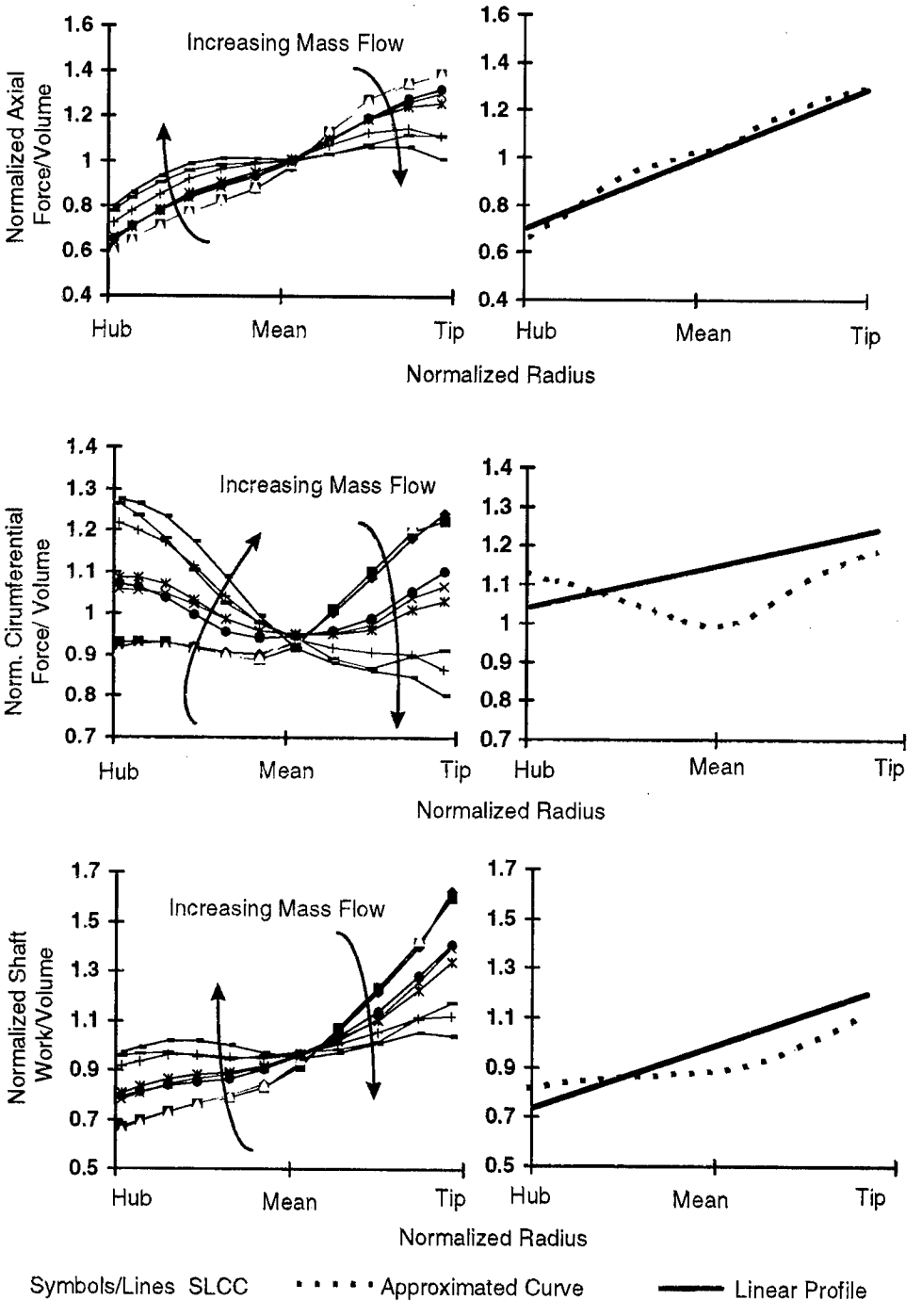

Figure 33. Source term correlation based on collapse in mass flow found from streamline curvature code solutions.

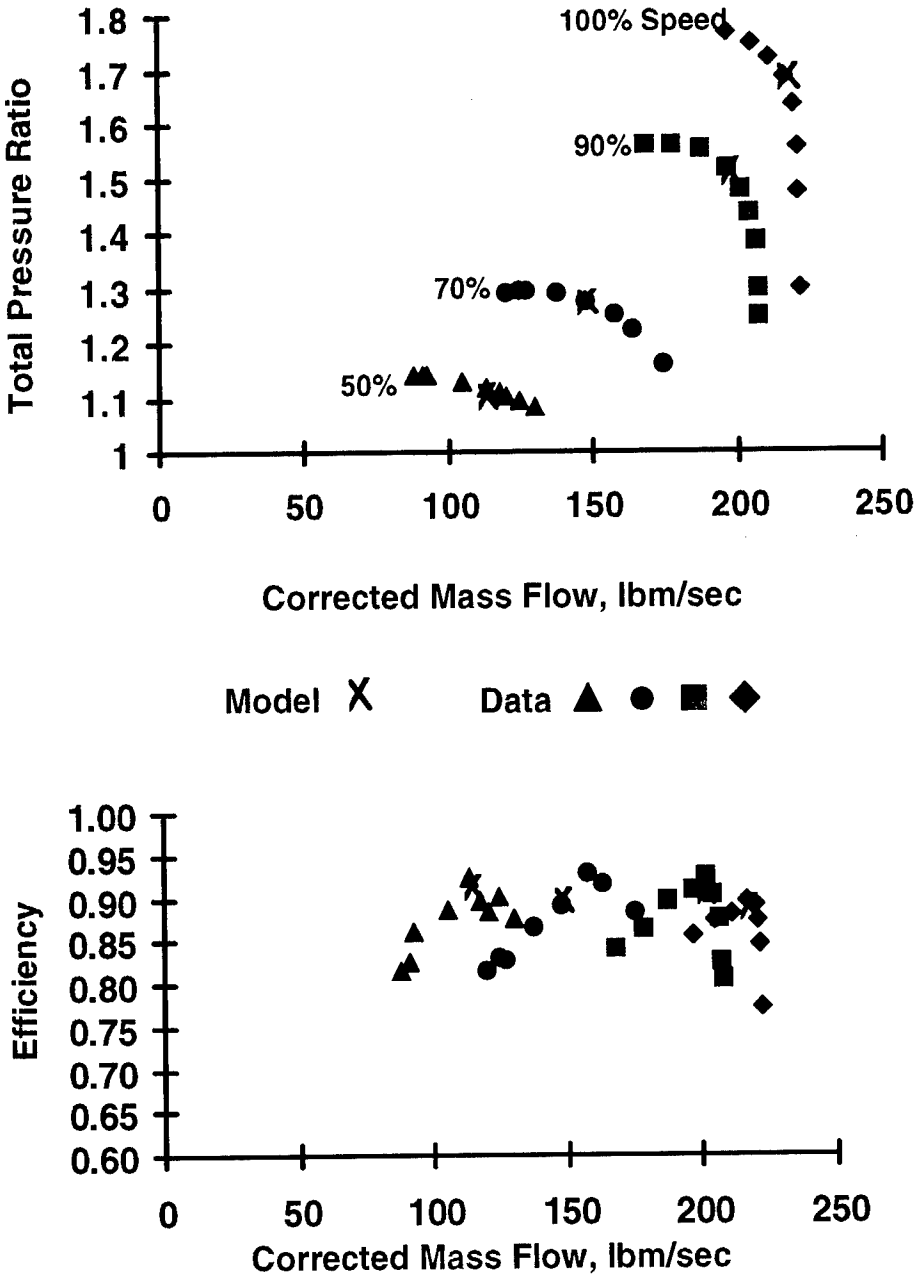

Figure 34. Overall constant throttle line performance using a linear radial distribution of sources based on a collapse in mass flow.

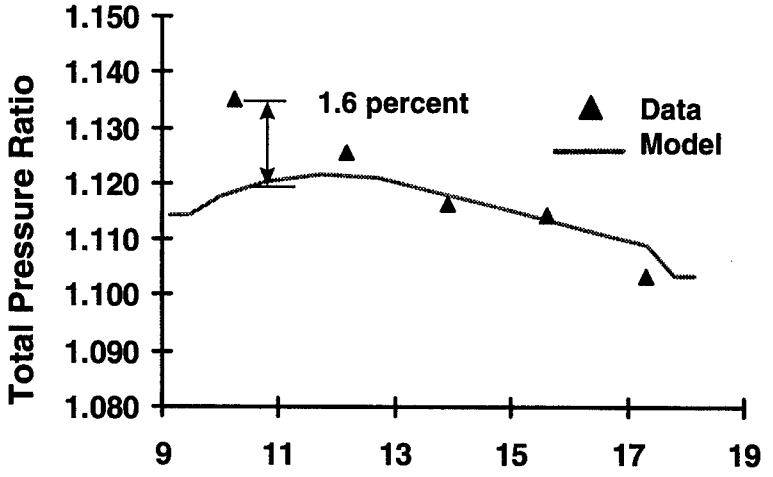

a. Total pressure ratio as a function of radius

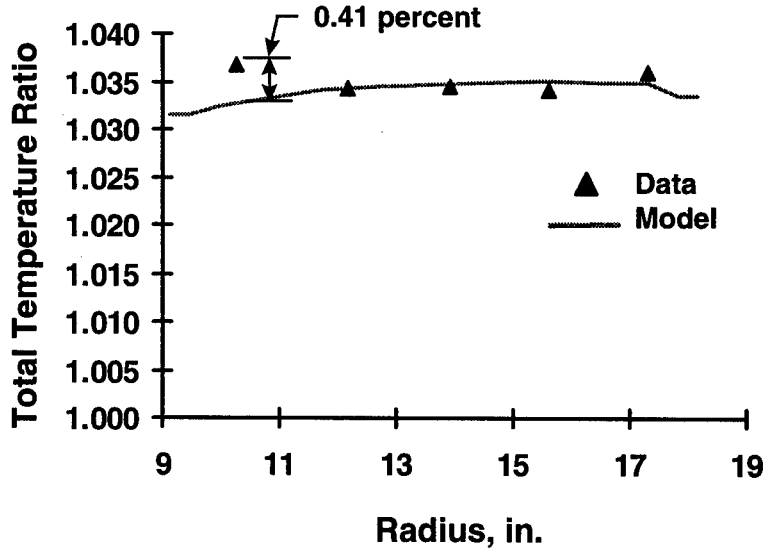

b. Total temperature ratio as a function of radius

Figure 35. Radial comparisons of results and experimental data on the constant throttle line at 50-percent speed using a linear radial distribution of sources based on a collapse in mass flow.

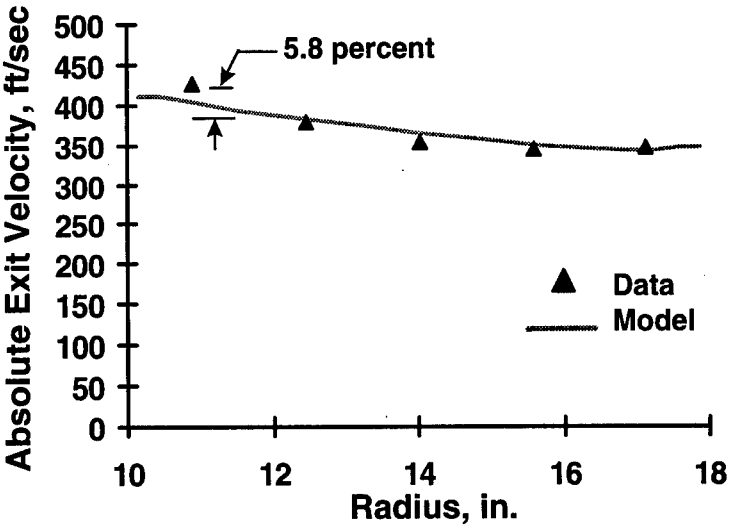

a. Absolute exit velocity as a function of radius

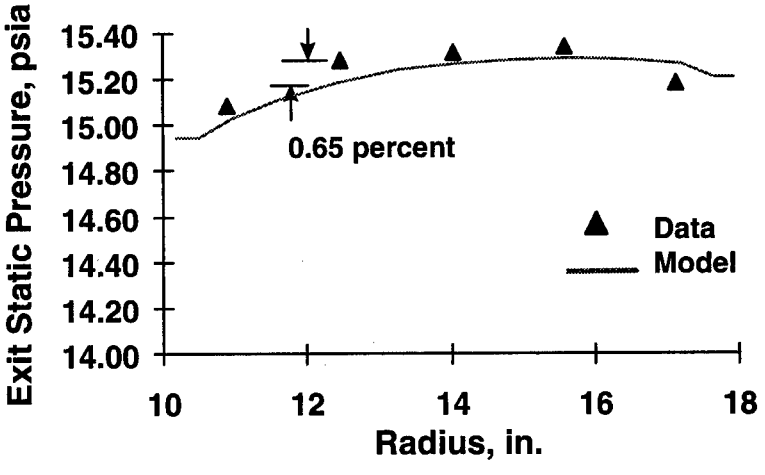

b. Exit static pressure as a function of radius

Figure 36. Additional typical radial comparisons of results and experimental data on the constant throttle line at 50-percent speed using a linear radial distribution of sources.

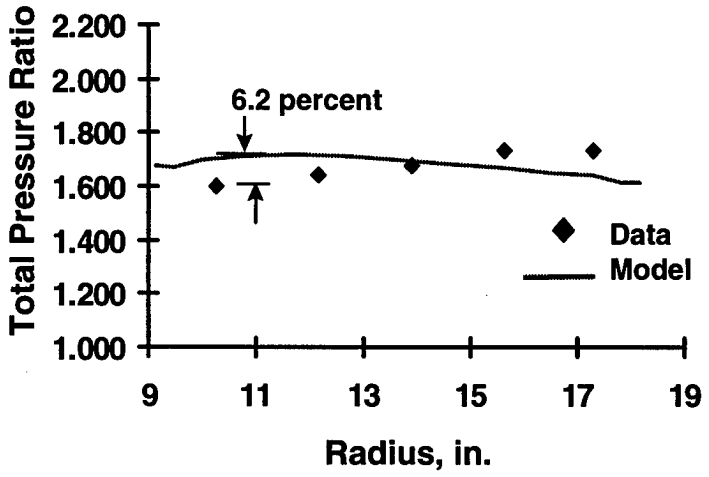

a. Total pressure ratio as a function of radius

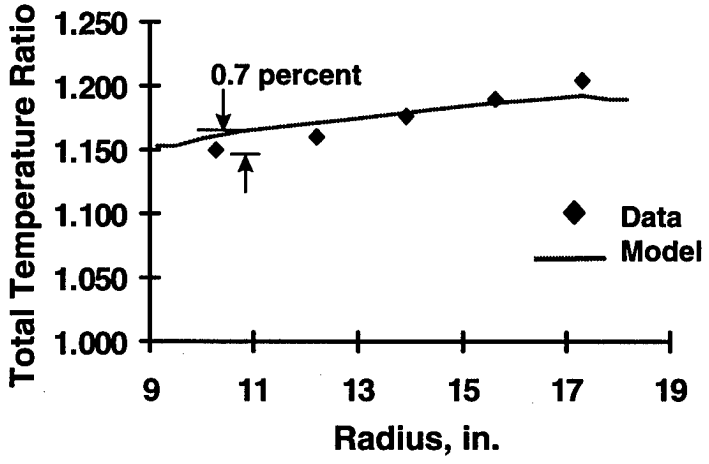

b. Total temperature ratio as a function of radius

Figure 37. Radial comparisons of results and experimental data on the constant throttle line at 100-percent speed using a linear radial distribution of sources based on a collapse in mass flow.

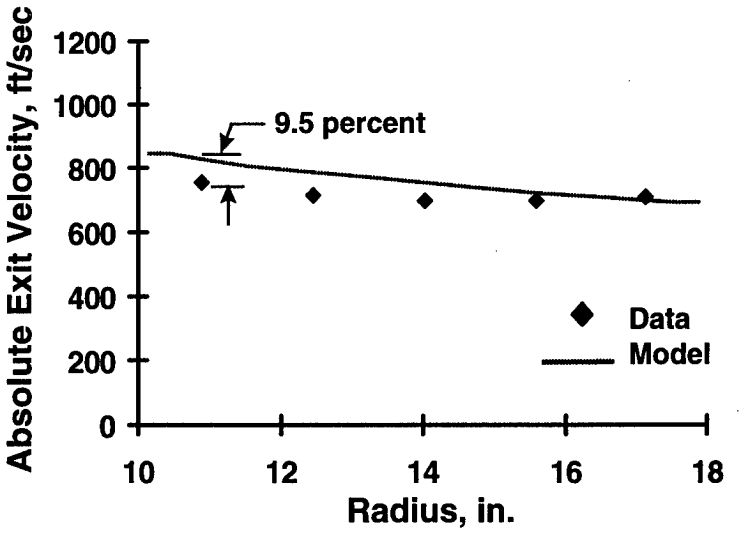

a. Absolute exit velocity as a function of radius

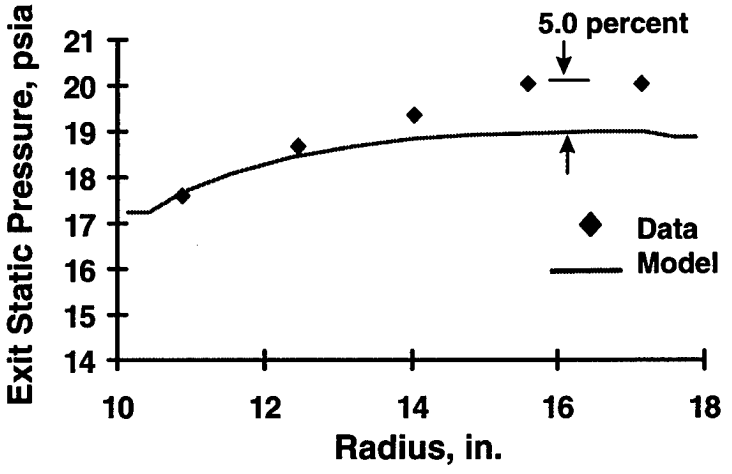

b. Exit static pressure as a function of radius

Figure 38. Additional typical radial comparisons of results and experimental data on the constant throttle line at 100-percent speed using a linear radial distribution of sources.

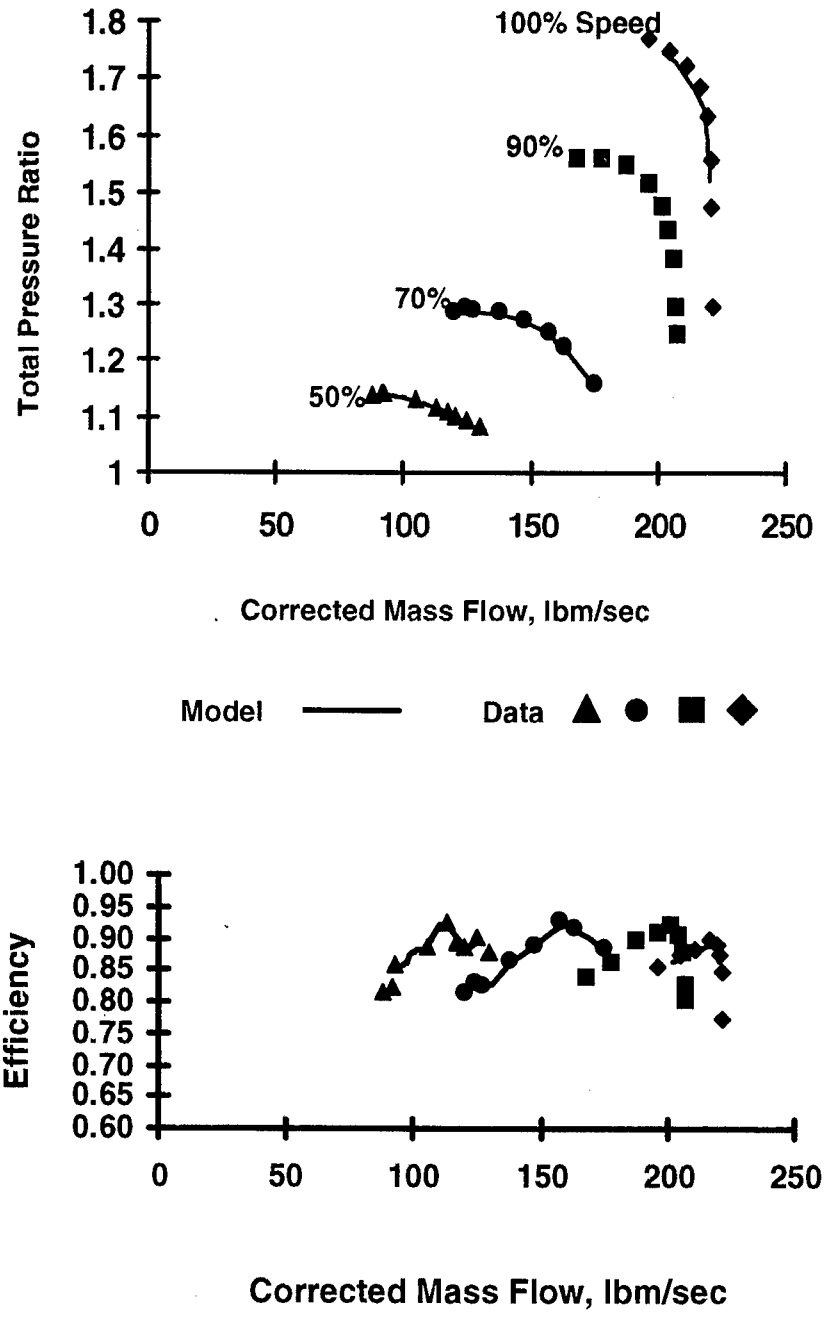

Figure 39. Overall performance map using a linear radial distribution of sources.

Table 1. Maximum Percent Difference Between Experimental Data and Simulation Results Along the Compressor Constant Throttle Line for Several Flow Parameters

Maximum Percent Differences from Experimental Data for 50-percent Speed						
Radial Method	Total Pressure Ratio	Total Temperature Ratio	Exit Mach Number	Absolute Exit Velocity	Exit Static Pressure	Static Temperature Ratio
Uniform	1.07	0.5	6.8	7.7	0.86	0.47
Interpolated	1.9	0.29	5.7	5.46	1.21	0.14
Linear	1.6	0.41	5.1	5.8	0.65	0.21

Maximum Percent Differences from Experimental Data for 70-percent Speed						
Radial Method	Total Pressure Ratio	Total Temperature Ratio	Exit Mach Number	Absolute Exit Velocity	Exit Static Pressure	Static Temperature Ratio
Uniform	4.29	1.17	8.2	7.4	2.1	5.45
Interpolated	1.7	1.08	4.7	5.0	0.9	0.3
Linear	1.5	0.42	5.5	4.8	0.89	1.39

Maximum Percent Differences from Experimental Data for 90-percent Speed						
Radial Method	Total Pressure Ratio	Total Temperature Ratio	Exit Mach Number	Absolute Exit Velocity	Exit Static Pressure	Static Temperature Ratio
Uniform	10.8	1.9	15.9	14.7	5.9	1.22
Interpolated	4.6	1.4	10.6	10.1	1.23	1.16
Linear	3.8	0.5	5.9	4.9	3.0	0.28

Maximum Percent Differences from Experimental Data for 100-percent Speed						
Radial Method	Total Pressure Ratio	Total Temperature Ratio	Exit Mach Number	Absolute Exit Velocity	Exit Static Pressure	Static Temperature Ratio
Uniform	12.5	2.17	15.4	16.1	8.9	4.9
Interpolated	28.0	1.09	28.6	29.0	3.9	4.4
Linear	6.2	0.7	9.8	9.5	5.0	3.7

APPENDIX A
NON-DIMENSIONALIZATION OF TURBOMACHINERY SOURCE TERMS

In order to include the turbomachinery source terms in NPARC, they had to be non-dimensionalized. In order to derive the appropriate non-dimensionalization parameters, the conservation equations were written in partial differential form as follows:

$$\frac{\partial \rho}{\partial t} + \ldots = W_B \tag{A-1}$$

$$\frac{\partial (\rho u)}{\partial t} + \ldots = F_x \tag{A-2}$$

$$\frac{\partial E}{\partial t} + \ldots = SW \tag{A-3}$$

Following the non-dimensionalization procedures used in NPARC, the non-dimensionalized equations were written in the same format:

$$\frac{\partial \bar{\rho}}{\partial \bar{t}} + \ldots = S_C \tag{A-4}$$

$$\frac{\partial (\overline{\rho u})}{\partial \bar{t}} + \ldots = S_x \tag{A-5}$$

$$\frac{\partial \bar{E}}{\partial \bar{t}} + \ldots = S_E \tag{A-6}$$

The conservation variables were non-dimensionalized using the standard NPARC methods:

$$\bar{\rho} = \frac{\rho}{\rho_{ref}} \quad ; \quad \overline{\rho u} = \frac{\rho u}{\rho_{ref} a_{ref}} \quad ; \quad \bar{E} = \frac{E}{\rho_{ref} a_{ref}^2} \quad ; \quad \bar{t} = \frac{t}{X/a_{ref}} \tag{A-7}$$

where X is a characteristic length. These non-dimensionalized variables were substituted into the left side of the conservation equations as follows:

$$\frac{\partial \rho}{\partial t} = \frac{\partial (\bar{\rho}\, \rho_{ref})}{\partial (\bar{t}\, X/a_{ref})} = \frac{\partial \bar{\rho}}{\partial \bar{t}} \frac{\rho_{ref} a_{ref}}{X} \tag{A-8}$$

$$\frac{\partial(\rho u)}{\partial t} = \frac{\partial\left(\overline{\rho u}\,\rho_{ref} a_{ref}\right)}{\partial\left(\bar{t}\,X/a_{ref}\right)} = \frac{\partial\left(\overline{\rho u}\right)}{\partial \bar{t}}\,\frac{\rho_{ref} a_{ref}^2}{X} \tag{A-9}$$

$$\frac{\partial E}{\partial t} = \frac{\partial\left(\overline{E}\,\rho_{ref} a_{ref}^2\right)}{\partial\left(\bar{t}\,X/a_{ref}\right)} = \frac{\partial \overline{E}}{\partial \bar{t}}\,\frac{\rho_{ref} a_{ref}^3}{X} \tag{A-10}$$

Substituting for the partial derivatives from Eqs. (A-1 - A-3) and Eqs. (A-4 - A-6) above produced

$$W_B = S_C\,\frac{\rho_{ref} a_{ref}}{X} \tag{A-11}$$

$$F_x = S_x\,\frac{\rho_{ref} a_{ref}^2}{X} \tag{A-12}$$

$$SW = S_E\,\frac{\rho_{ref} a_{ref}^3}{X} \tag{A-13}$$

Finally, solving for the non-dimensionalized sources yielded:

$$S_C = W_B\,\frac{X}{\rho_{ref} a_{ref}} \tag{A-14}$$

$$S_x = F_x\,\frac{X}{\rho_{ref} a_{ref}^2} \tag{A-15}$$

$$S_E = SW\,\frac{X}{\rho_{ref} a_{ref}^3} \tag{A-16}$$

X was assumed to be one, and the non-dimensionalizing parameters for forces in the y- and z-directions were easily deduced from the parameter derived from the axial momentum equation:

$$S_y = F_y\,\frac{X}{\rho_{ref} a_{ref}^2} \tag{A-17}$$

$$S_z = F_z\,\frac{X}{\rho_{ref} a_{ref}^2} \tag{A-18}$$

Equations (A-14 - A-18) show the appropriate combinations of reference density and reference speed of sound for non-dimensionalizing each of the turbomachinery source terms for implementation into NPARC.

NOMENCLATURE

a	Speed of sound
A	Cross-sectional area
B	1-D dependent variable matrix
C	1-D flux term variable matrix
d	Weights describing axial profile of sources
D	1-D source term variable matrix
e	Specific energy
E, **E**	Total energy, 3-D flux term variable matrix
F, **F**	Force, 3-D flux term variable matrix
G	3-D flux term variable matrix
H	Total enthalpy
J	Axial index in computational space
K	Radial index in computational space
L	Circumferential index in computational space
$\vec{n}$	Unit normal vector
P, $\mathcal{P}$	Pressure, Power
PR	Total pressure ratio
Q, **Q**	Heat-transfer rate, 3-D dependent variable matrix
r	Radius
R	Gas constant for air
S, **S**	Non-dimensionalized source term, 3-D source term variable matrix

SW	Shaft work
t, $\bar{t}$	Time, Non-dimensionalized time
T	Temperature
TR	Total temperature ratio
u	X-component of velocity
U	1-D axial velocity
v, v′	Y-component of velocity, Circumferential (tangential) velocity
V, $\vec{V}$, $\forall$	Total velocity, Velocity vector, Volume
w	Z-component of velocity
W	Mass flow rate
x	Cartesian physical spatial coordinate
X	Characteristic length
y	Cartesian physical spatial coordinate
z	Cartesian physical spatial coordinate

Greek

δ	Axial distribution function used in the weighting function
Φ	Compressor flow coefficient
γ	Ratio of specific heats
Γ	Torque
η	Transformed computational spatial coordinate
φ	Relaxation factor on sources
λ	Axial weighting function

θ	Absolute angle at circumferential location
ρ	Density
τ	Time constant, Transformed computational time
ω	Rotor rotational speed
ξ	Transformed computational spatial coordinate
Ψ	Compressor characteristic coefficients
ζ	Transformed computational spatial coordinate

Subscript

avg	Average or mean value
B	Bleed
C	Relating to continuity equation
cor	Corrected
e	Exit
E	Relating to energy equation
i	Inlet

Symbol Definition

j	Index in axial direction
k	Index in radial direction
L	Index in circumferential direction
max	Maximum value
r	Radial direction
ref	Reference quantity

ss	Steady state
t	Total
x	X- (axial) direction in Cartesian coordinates, Per unit length
y	Y-direction in Cartesian coordinates
z	Z-direction in Cartesian coordinates
θ	Circumferential (tangential) direction

Superscript

P	Pressure
T	Temperature
o	Previous or old value